ISSN 1999-656X

Iraqi Journal of Applied Physics Letters

VOLUME (4) ISSUE (3) JULY-SEPTEMBER 2021

Sponsored and Published by
Iraqi Society for Alternative and Renewable Energy Sources and Techniques

Co-published by
American Quality for Scientific Publishing

IRAQI JOURNAL OF APPLIED PHYSICS LETTERS

The *Iraqi Journal of Applied Physics Letters (IJAPLett)* is a peer reviewed journal of high quality devoted to the publication of original research papers from applied physics and their broad range of applications. IJAPLett publishes quality original research letters in physics and its applications in the broadest sense. It is intended that the journal may act as an interdisciplinary forum for physics and its applications. Innovative applications and material that brings together diverse areas of physics are particularly welcome. IJAPLett aims to disseminate knowledge; provide a learned reference in the field; and establish channels of communication between academic and research experts, policy makers and executives in industry, commerce and investment institutions. IJAPLett is a quarterly specialized periodical dedicated to publishing original letters in: Applied & Nonlinear Optics, Applied Mechanics & Thermodynamics, Digital & Optical Communications, Electronic Materials & Devices, Laser Physics & Applications, Plasma Physics & Applications, Quantum Physics & Spectroscopy, Semiconductors & Optoelectronics, Solid State Physics & Applications, Alternative & Renewable Energy, and Environmental Science & Technology.

ISSN (Print): 1999-656X, ISSN (Online): 2958-6488

EDITORIAL BOARD

Editorial Office:
P. O. Box 55259, Baghdad 12001, IRAQ
Website: www.iraqiphysicsjournal.com
Emails: editor@iraqiphysicsjournal.com, editor_ijap@yahoo.co.uk, ijap.editor@gmail.com,

ADVISORY BOARD

SPONSORED BY
IRAQI SOCIETY FOR ALTERNATIVE AND RENEWABLE ENERGY SOURCES AND TECHNIQUES (I.S.A.R.E.S.T.)
P. O. Box 55259, Baghdad 12001, IRAQ

PUBLISHED BY
AMERICAN QUALITY FOR SCIENTIFIC PUBLISHING INC.
1479 South De Gaulle Ct, Aurora,
CO 80018, United States

IRAQI JOURNAL OF APPLIED PHYSICS LETTERS

ISSN (Print): 1999-656x, ISSN (Online): 2309-1673

INSTRUCTIONS TO AUTHORS

CONTRIBUTIONS

Contributions to be published in this journal should be original research letters, i.e., those not already published or submitted for publication elsewhere, communications or letters to editor.
Manuscripts should be submitted to the editor at the mailing address:

Iraqi Journal of Applied Physics Letters, Editorial Board, P. O. Box 55259, Baghdad 12001, IRAQ
Website: www.iraqiphysicsjournal.com
Email: editor@iraqiphysicsjournal.com, editor_ijap@yahoo.co.uk, ijap.editor@gmail.com

MANUSCRIPTS

Two hard copies with soft Word copy on a CD or DVD should be submitted to Editor in the following configuration:

- **One-column** Double-spaced one-side A4 size with 2.5 cm margins of all sides
- Times New Roman font (16pt bold for title, 14pt bold for names, 12pt bold for headings, 12pt regular for text)
- Manuscripts presented in English only are accepted.
- Total number of words not exceed 2500 words and English abstract not exceed 100 words
- 4 keywords (at least) should be maintained on (PACS preferred)
- Author(s) should express all quantities in SI units
- Equations should be written in equation form (*italic* and symbolic) NOT in plain text
- Tables and Figures should be separated from text and placed in new pages after the references
- Charts should be indicated by the software used for generating them (e.g., Excel, MATLAB, Grapher, etc.)
- Figures and diagrams can be submitted in original colored forms for assessment and they will be returned to authors after provide printable copies
- Only original or high-resolution scanner photos are accepted
- For electronic submission, articles should be formatted with MS-Word software.

AUTHOR NAMES AND AFFILIATIONS

It is IJAPLett policy that all those who have participated significantly in the technical aspects of a paper be recognized as co-authors or cited in the acknowledgments. In the case of a paper with more than one author, correspondence concerning the paper will be sent to the first author unless staff is advised otherwise.
Author name should consist of first name, middle initial, last name. The author affiliation should consist of the following, as applicable, in the order noted:
- Company or college (with department name or company division), Postal address, City, Governorate or State, zip code, Country name, contacting telephone number, and e-mail

REFERENCES

The references should be brought at the end of the article, and numbered in the order of their appearance in the paper. The reference list should be cited in accordance with the following examples:
[1] X. Ning, R. Benford and M.R. Lovell, "On the Sliding Friction Characteristics of Unidirectional Continuous FRP Composites", *J. Tribol. Func. Mater.*, 124(1) (2002) 5-13.
[2] M. Barnes, "Stresses in Solenoids", *J. Appl. Phys.*, 48(5) (2001) 2000–2008.
[3] J. Jones, **"Contact Mechanics"**, Cambridge University Press (Cambridge, UK) (2000), Ch.6, p.56.
[4] Y. Lee, S.A. Korpela and R. Horne, "Structure of Multi-Cellular Natural Convection in a Tall Vertical Annulus", Proceedings of 7th International Heat Transfer Conference, U. Grigul et al., eds., Hemisphere (Washington DC), 2 (1982) 221–226.
[5] M. Hashish, "Waterjet Technology Development", High Pressure Technology, PVP-Vol. 406 (2000) 135-140.
[6] D.W. Watson, "Thermodynamic Analysis", ASME Paper No. 97-GT-288 (1997).
[7] C.Y. Tung, "Evaporative Heat Transfer in the Contact Line of a Mixture", Ph.D. thesis, Rensselaer Polytechnic Institute, Troy, NY (1982).

PROOFS

Authors will receive proofs of papers and are requested to return one corrected copy as a WORD file on a compact disc (CD) or by email. New materials inserted in the original text without Editor's permission may cause rejection of paper unless the handling editor is informed.

COPYRIGHT FORM

Author(s) will be asked to sign the IJAPLett Copyright Form and hence transfer copyrights of the article to the Journal soon after acceptance of it. This will ensure the widest possible dissemination of information.

OFFPRINTS

Authors will receive electronic offprint free of charge and any additional reprints can be ordered.

SUBSCRIPTION AND ORDERS

Annual fees (4 issues per year) of subscription are:
50 US$ for individuals inside Iraq; **200** US$ for institutions inside Iraq;
100 US$ for individuals abroad; **300** US$ for institutions abroad.

Structural Properties of Nickel Oxide Nanostructures Prepared by Induced Plasma Technique

Omar A. AL Rhhauy[1], K.H. Razyg[2], Kadhim A. Aadim[3]

[1] Department of Physics, College of Education for Pure Sciences, Tikrit University, IRAQ
[2] Department of Physics, College of Science, University of Baghdad, Baghdad, IRAQ

Abstract
In the current study, nickel oxide nanoparticles were made from bulk structure using the induced plasma process and various bombardment periods. These nanoparticles were created as thin layers on various thicknesses of glass substrates (prepared at different times of shelling). After that, they were analyzed with an x-ray spectrum, scanning electron microscope, atomic force microscope, and UV-visible spectrophotometer. When the optical constants and characteristics were measured, the films' energy gaps ranged from 1.85 eV to 2.1 eV depending on the bombardment periods. The AFM and SEM examination tools clearly reveal a structural change where the roughness varies with bombardment time due to the variation in the diameter of the nanoparticles. Finally, layers are completely crystalline by the x-ray spectrum.

Keywords: Induced plasma; Optical properties; Structure properties; Energy gap; Roughness
Received: 9 July 2020; **Revised:** 16 September 2020; **Accepted:** 23 September 2020; **Published:** 1 July 2021

1. Introduction

Nickel is a chemical element with atomic number 28, a shiny silver-white metal with a touch of gold. Nickel is a transition metal hard and malleable [1]. However, only small amounts of nickel are found in the atmosphere [2]. Within large nickel-iron meteorites that are not exposed to oxygen outside the Earth's atmosphere. It is believed that a mixture of iron and nickel forms the outer shell of the planet [3,4]. Nickel has many uses, especially in alloys. This includes the rapidly growing battery industry as a vehicle for electric vehicles [5]. Nickel has many special uses in chemical manufacturing, such as hydrogenation catalysts, battery cathodes, dyes, and metal surface treatments [6]. Nickel is an essential nutrient for some microorganisms and plants that contain enzymes that use nickel as their active site [7]. Nickel has face center cub (f.c.c.) structure (Fig. 1), and it is an alloy of many metals, used in hundreds of industries in a variety of ways. It is considered one of the most famous minerals in human history. Initially, humans had great difficulty dealing with the bends of nickel because it was difficult.

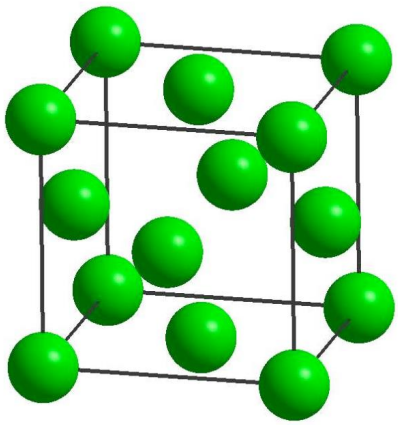

Fig. (1) Diagram showing the crystal structure of nickel [8]

Nickel is found in meteorites and can usually be found only in small quantities, but the largest source of it is in some ores, the minerals composed of iron, copper, and nickel. Perhaps this raw material is the most abundant source, since it is extracted and sent to most of the industrial regions of the world. As for how to extract it, the nickel-bearing ore is smelted in a high-temperature furnace, resulting in a fertile mixture or mixture of metals. This mixture turns into nickel by mixing it with coke and heating it in an oven at a high temperature. Nickel is known for its

shiny silver color and density, which is hard and malleable under heat. This means that it can be modified in the desired way and shape.

2. Process of Preparation

Using the induced plasma deposition approach, solutions containing nanoparticles were created for various preparation times 4, 6, 8 and 10 min. The nanoscale nickel has been obtained from 99% pure metal foils. The foils were cleaned with polishing paper and then washed with ethanol alcohol to get rid of any impurities on the metal's surface. Where the Ni metal before placing it in the glass beaker had dimensions of length and width of about 5 cm^2, after that, a part of the Ni metal was cut to about 1.5 cm^2. It will be submerged in a 10 ml beaker with 7 ml of distilled water, where the nozzle of the needle is directed in the middle of the metal. The metal foil will be linked to the positive electrode, while the negative electrode will be connected to the needle nozzle. If a needle nozzle is 7 cm from the target in order to produce a spark in the shape of a scattered blue flame. The process was carried out in the presence of argon gas that flows at a constant rate (3 L/s).

3. Results and Discussion

The induced plasma technique has been used to bombardment the nickel oxide particles for varying preparation times (bombardment) ranging at 4, 6, 8 and 10 min. Each solution's NiO particles' optical characteristics were recorded. The refractive index and the extinction coefficient both decline with wavelength in the range of 300–400 nm and then become remarkably stable for the other longer wavelengths. This change also occurs similarly in the optical constants for the same wavelength range. The energy band gap was 2 eV for the particles prepared at 4 min, 1.85 eV at 6 min, and subsequently increased to 1.88 eV and 2.1 eV for the particles prepared at 8 and 10 min, respectively. We can see that the energy gap widens as the grain size gets closer to the nanoscale. Table (2) shows the change of the grain size with time and table (3) energy gap with time.

Atomic force microscopy profiles shown in Fig. (2) demonstrate how grain size varies with preparation time and decreases with deposition time, which is consistent with an x-ray spectrum in which the peaks have shifted to the blue region. Additionally, the roughness of the surface diminishes with the bombardment time (table 1). The grain size decreases with bombardment period as in table (2), and this agree with AFM results.

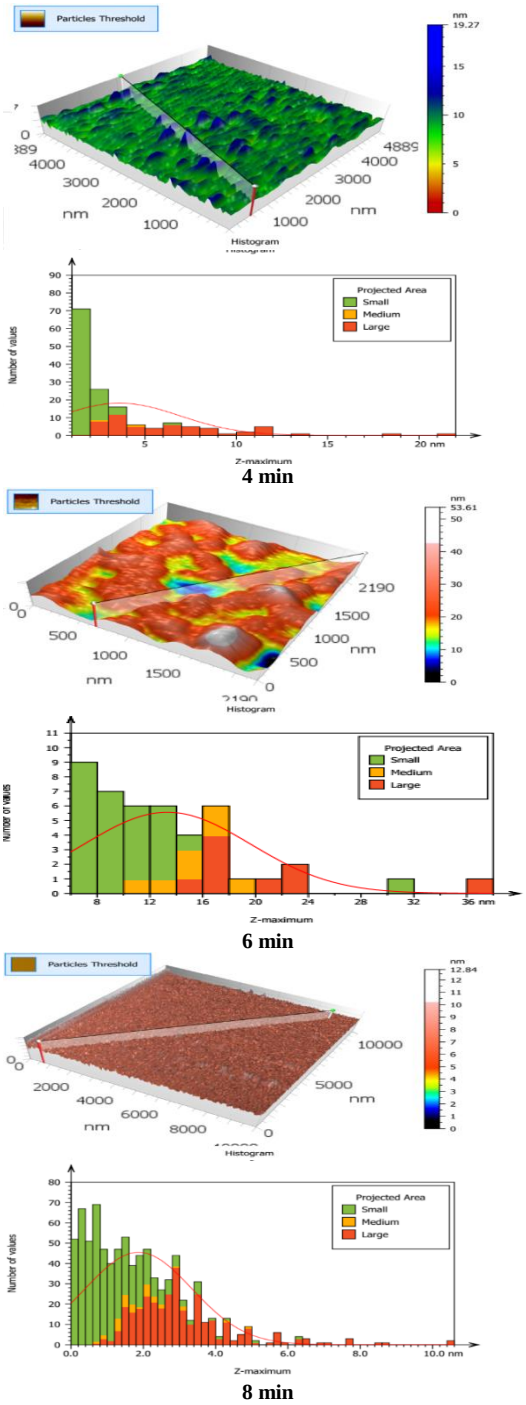

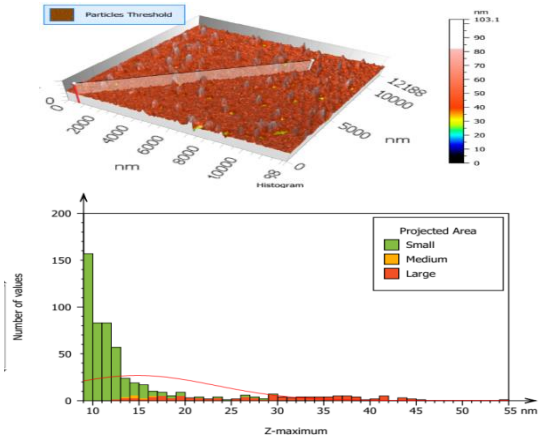

10 min

Fig. (2) Structural properties of CdO after induced Plasma bombardment for different bombardment periods (4, 6, 8 and 10 min)

Table (1) Data and energy gaps for AFM for ready samples at different bombardment times

Bombardment Time (min)	Surface Thickness (nm)	Roughness Average (nm)
4	1.095	1.317
6	2.75	7
8	0.47	0.122
10	4.322	9.17

Table (2) Average grain size for different bombardment time

Bombardment Time (min)	Average grain Size (nm)
4	3.36
6	3.3
8	3.3
10	3.67

Table (3) Energy band gap of the CdO prepared at different bombardment times

Bombardment time (min)	Energy gap (eV)
4	2
6	1.85
8	1.88
10	2.1

SEM images show that the grain size decreases with bombardment time as shown in Fig. (3), and this agree with AFM results.

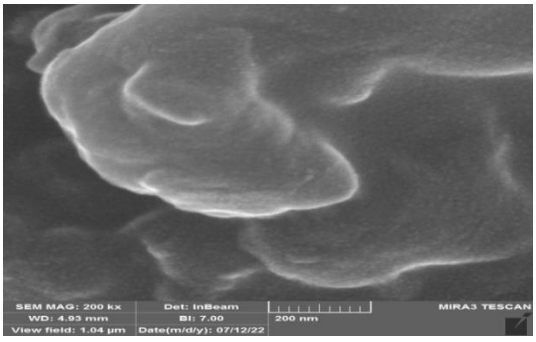

4min

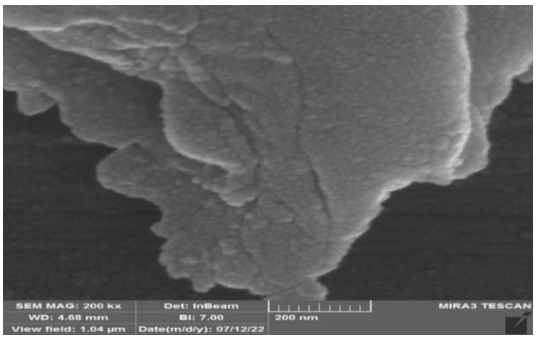

6 min

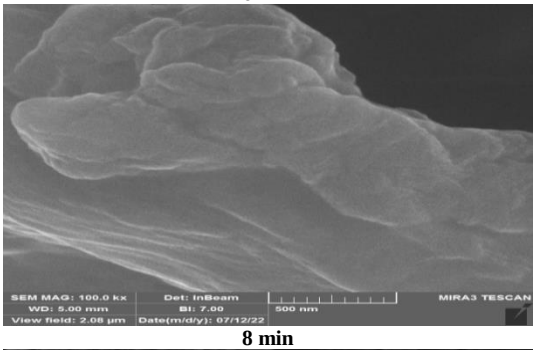

8 min

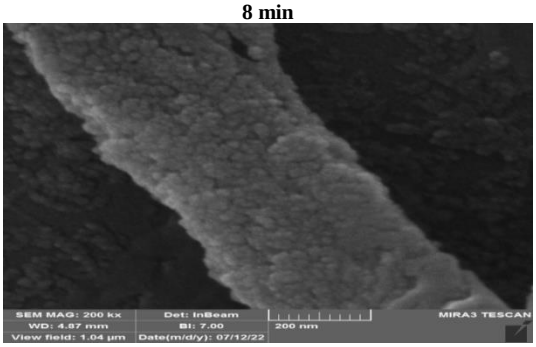

10 min

Fig. (3) SEM images of CdO prepared at different bombardment periods (4,6,8,10)min

An ionized gas called plasma has roughly equal amounts of positively and negatively charged ions and electrons [9]. Neutral atoms may be present in plasma. The plasma is referred to as partially or insufficiently ionized in this situation. If not, the plasma is referred to as totally or completely ionized [10]. The total number of positively and negatively charged particles in a partially or completely charged plasma must be balanced in order for the plasma to remain in a neutral state. The behavior and utility of plasma are frequently determined by interactions between the charged particles and the neutral particles. A plasma can have a wide range of properties depending on the type of atoms present, the ratio of ionized to neutral particles, and the energy of the particles [11].

4. Conclusions

Cadmium oxide nanoparticles have been prepared using the plasma jet technique for different bombardment periods. AFM images show that the roughness and surface thickness decrease with bombardment periods, and this agrees with SEM images and the XRD patterns. The XRD patterns show that the layers are completely crystalline. The peaks for all periods appear at the same 2θ with different intensities. In addition, the calculated grain size decreases with periods from 5.4 to 3.5 nm. The optical properties and energy gap varied clearly with bombardment periods.

References

[1] Nickel: Nickel Metal Information and Data". Mindat.org . Archived from the original on March 3, 2016. Retrieved March 3, 2016. Retrieved March 2, 2016

[2] Sticksrud, Lars; Wasserman, Yevgeny; Cohen, Ronald (November 1997). Composition and temperature of the Earth's inner core. Journal of Geophysical Research. 102 (B11): 24729 - 24740. Bibcode: 1997JGR... 10224729S. doi: 10.1029/97JB02125.

[3] Coy, J. M.D.; Skomerev, F.; Gallagher, K.; (1999). "Rare Earth Metals: Is Gadolinium Really Magnetic?". nature . 401 (6748): 35-36. Bibcode: 1999Natur.401...35C. doi: 10.1038/43363. S2CID 4383791 .

[4] Nickel use in society". Nickel Institute. Archived from the original on September 21, 2017

[5] Treadgold, Tim. "Gold is hot but nickel is even hotter as demand for batteries in electric vehicles increases". Forbes. Retrieved October 14, 2020.

[6] Nickel Compounds - The Inside Story". Nickel Institute.

[7] Archived from the original on August 31, 2018.

[8] Liu, P., Chen, D., Wang, Q., Xu, P., Long, M., & Duan, H. (2019). Crystal structure and mechanical properties of nickel–cobalt alloys with different compositions: A first-principles study. Journal of Physics and Chemistry of Solids, 109194. doi:10.1016/j.jpcs.2019.109194.

[9] مصدر البطاقة

[10] N . Braithwaite, “Introduction to gas discharges” Plasma Sources Sci. Technol. 9 517–527,(2000).

[11] J. Diedrich," Laser-Induced Breakdown Spectroscopy on Bacterial Samples", M.Sc. thesis, Wayne State University USA, (2007).

[12] K.H. Spatschek, "Introduction to Theoretical Plasma Physics", lecture series, (2008).

Computer-Aided Design of New Immersion Magnetic Lens

R.Y.J. AL-Salih, Othman M.A. AL-Bayati

Department of physics, College of Sciences, University of Tikrit, Salahaddin, IRAQ

Abstract

New design of an objective magnetic immersion lens has been studied, where three innovative designs of immersion lenses were developed in a variable manner in the geometric dimensions. The axial magnetic field of these lenses was calculated by the Finite Element Method and using computer programs to study the focal properties of these lenses. L1, L2, L3 and it was found that the L3 lens achieved the best results because it had the lowest values of focal length, which corresponds to the highest values of the magnetic field, and had the lowest values of spherical aberration coefficients Cs and chromaticity Cc at a constant value of the irritant factor (NI=4800 (A-t).

Keywords: Magnetic lens; Immersion lens; Magnetic properties; Optical properties; Electronic optics
Received: 10 July 2020; **Revised:** 17 September 2020; **Accepted:** 2 October 2020; **Published:** 1 July 2021

1. Introduction

Electronic optics is the mathematical framework for calculating and studying the behavior of the paths of the electronic beam and ways to control them along the electric and magnetic fields, and that the electron microscope is one of the most important applications of electronic optics [14]. It is the hypothesis developed by the French scientist Louis de Broglie in 1925 about the wave nature of moving particles. As for the second pillar, it is the experience of the German scientist Hans Bosch in 1926, who scientifically proved the possibility of focusing a beam of charged particles in one point after passing through an axially symmetrical magnetic field, which he called the electronic lens [1].It has become possible to know the distribution of magnetic and electric flux density and to calculate the optical properties of any proposed electronic lens before manufacturing [2].Therefore, computer simulations played an important role in designing and improving optical systems for charged particles. Therefore, we can predict the calculations and performance of these systems with high accuracy before they are manufactured, which contributed to Save a great deal of money and time [3]. The researcher (Abdullah) in 2005 proposed five forms of magnetic electronic lenses, each of these lenses has an iron circle and a coil of circular cross-section. The distribution of the axial magnetic flux density and the path of the magnetic flux lines inside those lenses were studied, as well as the objective and projective optical properties of those lenses were calculated, and it was concluded that the round magnetic lens produces a relatively high peak value for the distribution of the axial magnetic flux density and the paths of the regular magnetic flux lines. Moreover, it has relatively low objective focal characteristics of focal length, spherical and chromatic aberration. This type of lens can be used as an objective lens in transmission electron microscopy [4]. In 2021, Basma and Ahmed were able to design magnetic lenses with optimal operating conditions, as they presented a study on the effect of the diameter of the axial aperture and the air gap between the poles, as well as the thickness of the pole face on the magnetic and optical properties, and they found that the optical properties and the distribution of magnetic flux density improve with Reducing the diameter of the axial aperture as well as reducing the air gap between the poles of the symmetric monopolar magnetic lens. As for the thickness of the electrode face, they found that the best magnetic properties, the highest value of magnetic flux, the lowest value of the axial

magnetic field strength, and the narrowest bandwidth was when the thickness of the electrode face was equal to (4.3 mm) for the proposed design [5]. In 2021, Mardeen and Al-Jubouri studied the design of a immersed magnetic lens and it was found that the distance between the poles has a direct effect on the focal properties and found that the best distance between the poles is (2 mm) because they have the lowest values of focal length and beam diameter, which corresponds to the highest analysis value [15].

2. Theory Part

Magnetic lens is a tool used for the purpose of focusing or focusing a beam of particles that are affected by the magnetic field (electrons or ions) on a specific point [6].The objective magnetic lens is an important part of the scanning electron microscope because of its large and direct impact on the ability to analyze it, and for the purpose of reducing distortions. And defects that affect the purity and clarity of the image formed in the electron microscope, accuracy should be taken into account when designing this type of lens in order to obtain a distribution of high magnetic density B_{max} and thus optical properties such as focal length, spherical and chromatic aberrations [7]. The magnetic lens consists of a coil with Copper conduction wires and electrically isolated, the coil is placed inside an iron circuit that works to focus and confine the magnetic field in a narrow area called the magnetic pole, which is a small hole that allows electrons to pass along the optical axis, which works to form an image of the sample and prevents the iron circuit from leaking the magnetic field outside Lens [8]. In this research, a immersed magnetic objective lens will be designed in which the location of the sample is in the aperture between the poles inside the lens and Enter the magnetic field, One of the advantages of this lens is that the focal length is very small, and we get a high analysis of images, but it has many disadvantages, including a limitation in the sample size that does not exceed (5mm), and it is not possible to examine models that contain magnetic materials [9]. In this research, three models of immersion magnetic lenses were designed and then finding the magnetic flux density and magnetic flux lines and calculating the optical properties represented by the spherical aberration coefficient Cs, the chromatic aberration coefficient Cc and the focal length ˚F, then choosing the best model and the figures (1-3) showing the shapes and dimensions designs for lenses.

3. Experimental Part

The design of magnetic lenses requires determining the best geometric shape. Three models of the immersion magnetic lens were proposed, and then they were designed and named with the symbols L1, L2, L3, respectively. Figures (1-3) show a cross-section of the geometric dimensions of the three proposed lenses.

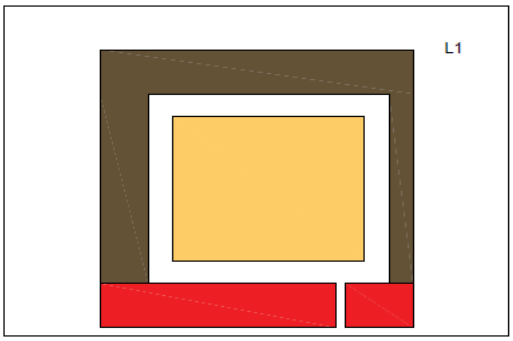

Fig. (1) First Design Lens (L1)

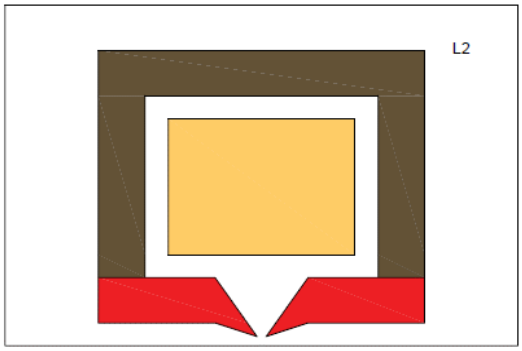

Fig. (2) Second Design Lens (L2)

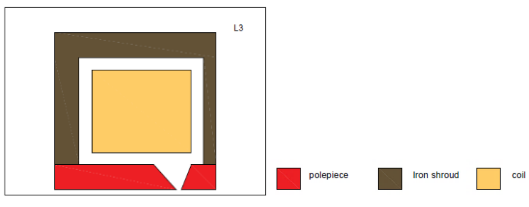

Fig. (3) Third Design Lens (L3)

The program (EOD) [10]. Based on the finite element method (FEM) was used to design a immersion magnetic lens, as the dimensions of the lens were determined for the purpose of calculating the axial magnetic field and its objective optical properties. In order to design a high-efficiency immersed lens, that lens must generate the highest peak magnetic flux density. The distribution of the axial magnetic flux density Bz was calculated for the proposed immersion magnetic lenses shown in the figures (4-6) in a two- and three-dimensional manner. Table (1) shows Summary of the electromagnetic analyzes of the three lenses at a constant value of coil irritation of (NI=4800 A.t). Figure (7) shows the difference in the distribution of the axial magnetic flux density for these lenses along the optical axis. It is noted that L3 achieves the best flux density than L1 and L2. Despite obtaining this clear detail for the values of the magnetic flux density distribution curves above, this result is still not enough to distinguish the best lens among these lenses because there are other very important properties that have not yet been studied such as the paths of magnetic flux lines and the objective focal properties that will be addressed Later. However, it can be said that this result is considered as an initial positive indicator for choosing the best lens at this stage of work.

Table (1) A summary of the electromagnetic analyzes of the three lenses when excited (NI=4800A.t)

Lens symbol	Pinpoint position Z (mm)	$B_{z\ max\ (Tasla)}$
L1	0	0.69
L2	1	0.85
L3	1	1.32

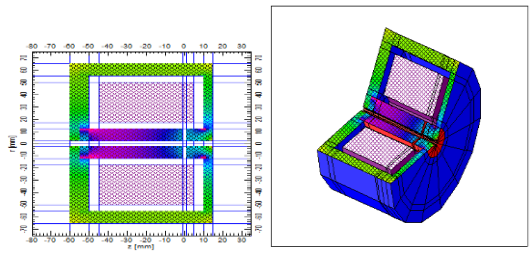

Fig. (4) First Lens (L1) (a) Two-dimensional (b) three-dimensional

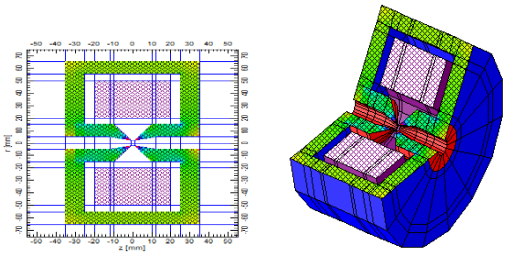

Fig. (5) Second Lens (L2) (a) Two-dimensional (b) three-dimensional

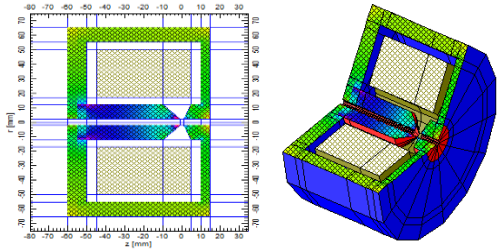

Fig. (6) Third Lens (L3) (a) Two-dimensional (b) three-dimensional

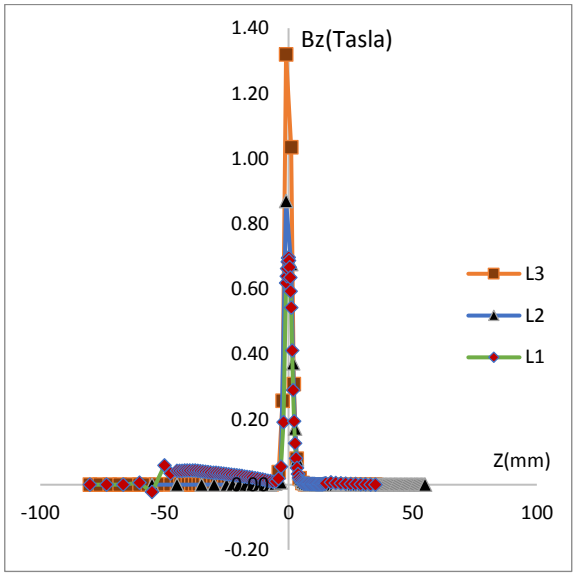

Fig. (7) Distribution of the axial magnetic flux density (B_z) as a function of distance (z) for the three proposed lenses when excited (NI=4800A.t)

Calculating the paths of the magnetic flux lines is of great importance in studying the behavior of lenses and knowing their optical performance, as well as knowing the magnetic leakage in their structures [11]. And in order to clarify the effect of the geometric shape on the paths of the magnetic flux lines of the lens, tests were conducted on all the proposed lenses using the (EOD) program to calculate the magnetic flux lines In the installation of magnetic lenses when both (Vr=10kV) and (NI=4800 A.t) are proven. The figures below show the 2d and 3d widths of the paths of the

magnetic flux lines within the installation of the three magnetic lenses that are different in design. Figures (8-10) show the concentration of magnetic lines with high intensity in areas that have high magnetic flux and less intensity in areas with low magnetic flux.

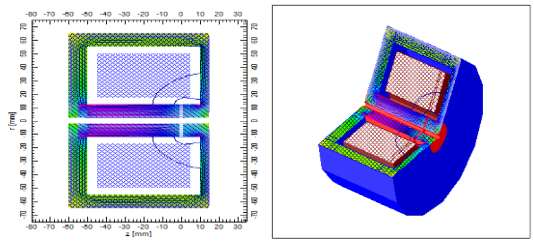

Fig. (8) The path of the magnetic flux lines of the lens L1

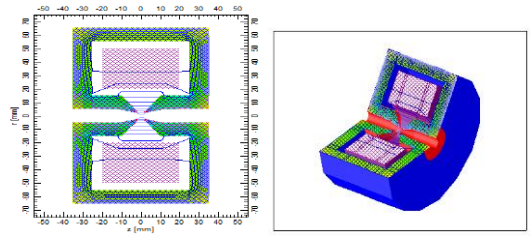

Figure (9) The path of the magnetic flux lines of the lens L2

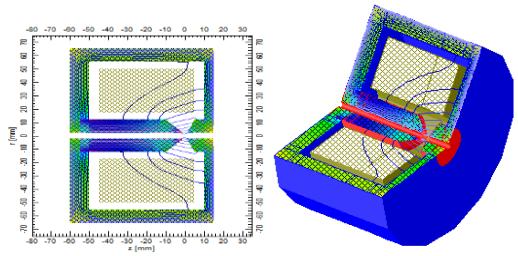

Fig. (10) The path of the magnetic flux lines of the lens L3

4. Conclusions

The symmetrical immersed magnetic objective lens, symbolized by L3 and shown in Figure (7), achieved the best results from the three proposed designs because it had the lowest values of the focal length that corresponded to the highest values in the analysis, and it had the lowest value for the spherical and chromatic aberration coefficients at a fixed value of the irritant factor (NI=4800 A.t).The change of the pole shape and the position of the pole head of the immersion magnetic lens directly affects the focal properties of the magnetic lens. L3 immersed magnetic objective lens has a maximum value of the axial magnetic flux density distribution (Bz max = 1.32 T) at the site (Z=1mm) when the lens is excited (NI=4800 A.t).

References

[1] S.A. Sultan and A.I. Alabdullah, "Effect of pole face thickness on magnetization of the single-pole magnetic lens", *Rafidain J. Sci.*, 29(4) (2020) 44-52.

[2] H.S. Hasan, S.A. Obaid and M.S. Erhayief, "Recent Development-2 of CADTEL Software: The Optimum Conditions of Scherzer Imaging in the Electron Magnetic Lenses," *Iraqi J. Sci.*, ?? (2022) 131-148.

[3] H.S. Hasan, S.A. Obaid and M.S. Erhayief, "Munro's Electron Beam Software MEBS," Report, MEBS Ltd. (London, 2011).

[4] A.E Al-Abdullah, "The Electron Optical Properties of the Round Magnetic Electron Lens," *Rafidain J. Sci.*, 17(3) (2006) 59-69.

[5] B.F. Abd Alghane and A.K. Ahmad, "Design of symmetric magnetic lenses with optimum operational conditions," *Al-Nahrain J. Sci.*, 24(1) (2021) 30-38.

[6] M. Szilagyi, **"Electron and Ion Optics"**, Springer Science & Business Media (2012).

[7] J. Podbrdský, "High current density magnetic electron lenses in modern electron microscopes," *Scan. Electron Microsc.*, 1986(3) (1986) p. 8.

[8] P.W. Hawkes, **"Magnetic Lens Theory",** in Magnetic Electron Lenses, Springer (1982) 1-56.

[9] J. Pawley and H. Schatten, **"Biological Low-Voltage Scanning Electron Microscopy"**, Springer (2007).

[10] T.M. Abbas and Q.A. Sahi, "Design and Study of The Optical Properties of Electromagnetic lenses Dual-polar analog using the program I", *J. Univ. Babylon Pure Appl. Sci.*, 25(6) (2017) 1991-1997.

[11] T. Mohsen and L. Merry, "Studying the Properties of the Magnetic Optical Lenses by Using Mathematical Functions", *Int. J. Eng. Res.*, 3(7) (2014) ??-??.

[12] R.Y.J. Al-Salih, "The Influence of Bores Diameter on the SEM's Objective Lens Properties", *Tikrit J. Pure Sci.*, 23(2) (2018) 107-113.

[13] R.Y.J. Al-Salih, A.I.M. Al-Abdulla and E.M.A. Alkattan, "Simple program for computing objective optical properties of magnetic lenses", *Int. J. Comput. Appl. Technol.*, 66(3-4) (2021) 254-259.

[14] M.K. Al-Shammari, "Design and Improving the Optical Properties of a Magnetic Unipolar lens and Studying Its Geometric Parameters and Subjugation", MSc thesis, Tikrit University (2022) (not published).

[15] M.J. Ahmed, "Design and Fabrication the Objective Magnetic Lens in the Scanning Electron Microscope and Study its Optical Properties" MSc thesis, Kirkuk University (2021) (not published).

Structural Characteristics of Cadmium Oxide Thin Films Prepared by Chemical Bath Deposition

Alaa Y. Ali[1,2] Hasan H. Ali[2], Akram A. Khalaf[3], Abdullah M. Ali[2], Mustafaa Y. Ali[2], Amjad H. Jassim[2], Ahood Hassana, Mustafa K. Hawas[2], H. Yousif Alib

[1] Department of Energy, Natural Resources Research Centre, Tikrit University, Tikrit, IRAQ
[2] Department of Physics, College of Education for Pure Sciences, Tikrit University, Tikrit, IRAQ
[3] Department of Optics Techniques, Al Farabi University College, Baghdad, IRAQ

Abstract
Chemical bath deposition (CBD) has been involved in the preparation of films which are formation from Cadmium Oxide (CdO). Fabricated films were annealed at 300ºC with 0.03 M of concentration. The analysis of structure, morphology and optical were obtained in thin films. For characterization of heterojunction CdO/Si, the electrical properties were achieved for photodetector application. In structure analysis, X-ray diffraction (XRD) shows appearance of a phase identical with cubic of CdO film. Atomic force microscopy (AFM) characterised and viewed the shape of topography films. In addition, Scanning electronic microscopy (SEM) was shown the material structure on the surface. Moreover, the exhibition of films in optical properties was in maximum values of absorption wavelengths ~ 0.9 in the visible region of the spectrum. For more details, the estimation of band gap energy (E_g) was around 2.70 eV. These results were important and significant influence on the electrical properties of CdO/Si heterojunction. The material considered being a good oxide semiconductor for heterojunction application.

Keywords: Cadmium oxide; Thin films; Heterojunction; Photodetectors; Chemical bath deposition
Received: 13 July 2020; **Revised:** 25 August 2020; **Accepted:** 2 October 2020; **Published:** 1 July 2021

1. Introduction

Recently, the amazing deal of research is focused on the development of nanostructure materials for future applications. Several materials in nanotechnology field have been investigated to apply in necessary applications for human requirements. The improving of quality and low-cost nanomaterial is the interested subject of research centres around the world in nanoscience and nanotechnology field. However, the development in nanotechnology opens a new roadmap for synthesis of unique classes of nanomaterial with enhanced the industry applications. The metal oxide semiconductor considered to be a significant interest for industry and science filed relating to their advantage, like commercial material, availability, and small size selectivity.[1] Nanostructure oxides and controlling the particle size can be contribution in the demand of different fields of science. Sharma et al. have reported the composite thin film CdO-ZnO for gas sensor applications.[2] They have achieved the maximum response of 52.04% for 24 ppm for Ethanol at minimum operation temperature ~325°C. This application has realised a great idea for future development of nanostructure CdO-ZnO film. In CBD method, Buba et al. fabricated CdO films with carrier density (N) and conductivity (σ) of about $1.245X10^{22}$ cm^3, 0.69 Ω/m respectively. This achievement was at a high temperature annealed of 300ºC.[3] For sensitized solar cell application, ZnO was companioned in nanostructure photoanode in a CdS quantum dot [4]. More details in this work, it was a ZnO nanocones covered with ZnO nanospikes and employed as the photoanode in a CdS quantum dot-sensitized solar cell (QDSSC). The improvement contributed to reduce the recombination of the photoexcited electrons. ZnO/CdS was demonstrated as n-type semiconductor layer on the performance of ZnO/CdS/Cu(In,Ga)Se_2/Mo modules with monolithic interconnects [5]. ZnO and CdS were a part of the gate material that is contacted directly into the drain of the simplified model and this layer supported qualitatively the proposed mechanism in the device junction. In the nanostructure study, ZnO/CdS with ITO/TiO_2 nanofilm prepared

to involve in the photoelectrochemical analysis as heterostructure. Cd nanoparticles formatted on the surface of oxides materials and the nanostructure was obtained via the photochemical reduction method. The binary oxide CdO_x and ZnO_{1-x} nanoparticles achieved at different concentrations by thermal treatment technique [6].

2. Experimental Part

CdO thin films were prepared onto microscopic glass substrate utilizing CBD synthesis. Before preparation, glass substrates cleaned through the ultrasonically with ethanol and detergent. In the end of wishing process, substrates were rinsed in acetone and deionised (DI) water then dried in an oven. The cleaning process was carried out to make sure that the essentially surface of substrate is cleaned completely for nucleation centres of formation to deposit CdO films. For the deposition of CdO, Cadmium Chloride ($CdCl_2H_2O$) had use as precursor for preparation of the CdO thin films as Cd^{2+}ion source. 5ml of $CdCl_2$ utilized poured into a beaker followed by the gradual introduction of 30% NH_3 with slight shaking which was initially turns the solution white and odourless. More quantity of the NH_3 solution was added to about 4ml as demonstrated by Ezekoye et al. [16] and Lalithambika et al. [17] 34 ml of double water was added to the mixture which turns the solution fair white. The mixture has been kept in an open conical flask in order to acquire sufficient amount of oxygen. The pH of the bath had maintained at 9.5 confirming the alkalinity of the bath. Thereafter, the solution transferred back to the beaker ready for deposition process. The cleaned substrates were inserted into the reaction bath and held vertically in a synthetic foam cover which was left for 24 hours for the deposition to complete. The substrates were then withdrawn from the bath and rinsed with distilled water and allowed to dry in air. The samples were then annealed at temperature of 300^{o}C for 15 min.

XRD (XRD 6000-Shimadzu) is a significant technique to clarify the crystal structure and the crystalline phases. AFM (AA3000 - Angstrom Advanced Inc) and SEM (VEGA3-TESCAN model- USA) were viewed a deep analysis of surface samples. The thin films were characterised for their optical properties using UV-VIS Spectrophotometer UV-1800 while, the electrical characterisation of the samples was carried out by Keithley 619 electrometer with thermometer (Viicto-81B) for electrical conductivity measurement. For heterojunction photodetector, spectral responsivity was measured via a detection system (Infrared Spectroradiometer, Model 746) that used consisting of a light source and a uniform wavelength.

3. Results and Discussion

In the analysis materials, it is a scientific way to identify the element component material via X-ray diffraction (XRD) in first measurements (Fig. 1a). XRD can be clarified the crystallographic structure of CdO. This technique was utilised to study the crystalline formation of CdO deposited via CBD. XRD of CdO was shown a polycrystalline structure of cubic type with the best crystalline orientation (111) [18]. The appearance of additional peaks of (200) with the other peaks viewed the hydroxide represent the phase of CdO. The membrane patterns show a polycrystalline structure of cubic type at (111). The deposited films were examined via optical microscope to find out the nature of the surfaces with 10X (Fig. 1b). It appears that the surface of the membrane is greenish-yellow with a homogeneous arrangement of granules on the morphology of film. AFM was used to view the surface topography with more details of the prepared films. AFM analyses with two dimensions (2D) were homogeneity and regularity of samples surface (Fig. 1c). There are a large number of adsorbed grains lines up regularly on the surface of the sample without holes or intermittent assemblies of granules in the morphology structure. This indicates that the topography of surfaces have a high homogeneity and uniformity, which makes them suitable for semiconductor device applications such as photodetectors and solar cells.

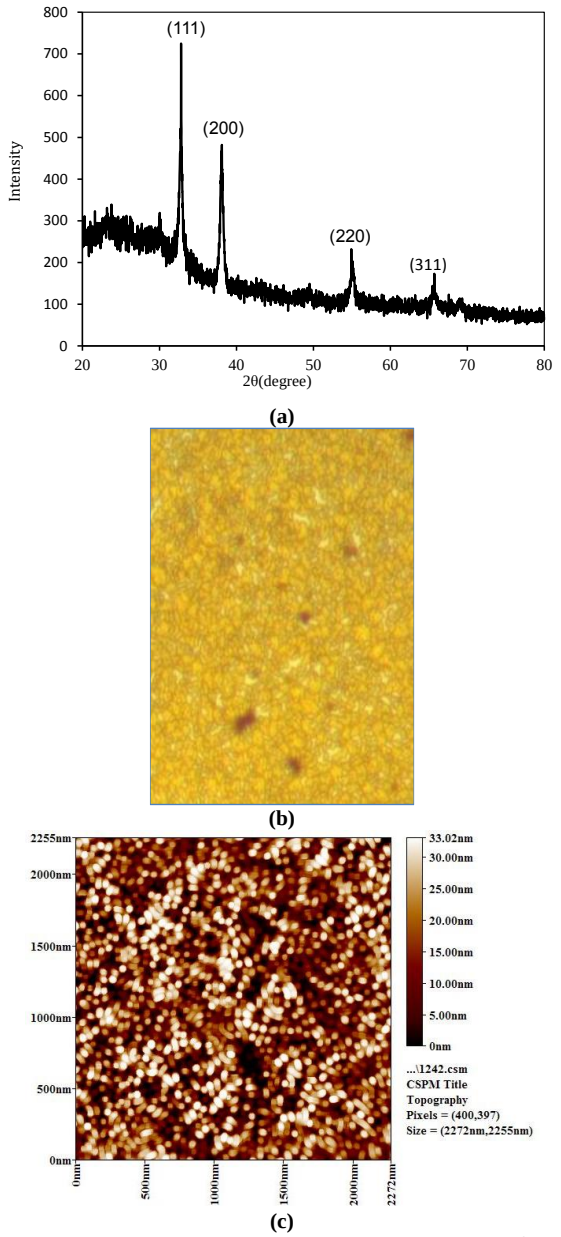

Fig. (1) (a) XRD pattern, (b) optical image and (c) AFM of CdO films

CdO films were examined using scanning electron microscopy (SEM) technology with a magnification of (2,000X) for the purpose of identifying the nature of the surface (Fig. 2a). The observing nanoparticles size was in the sedimentation and uniformly distributed granules of topography films. Energy-dispersive x-ray spectroscopy (EDS) analysis of the proportions elements in the prepared films after heat treatment, it noticed the appearance of the elements such us Cadmium and Oxygen (Fig. 2b). The measurement indicated the morphology of polycrystalline structure and the cubic type, which represents CdO. There was an appearance of small percentage of Carbon dioxide that is related to the presence of impurities inside the furnace during the heat treatment of films.

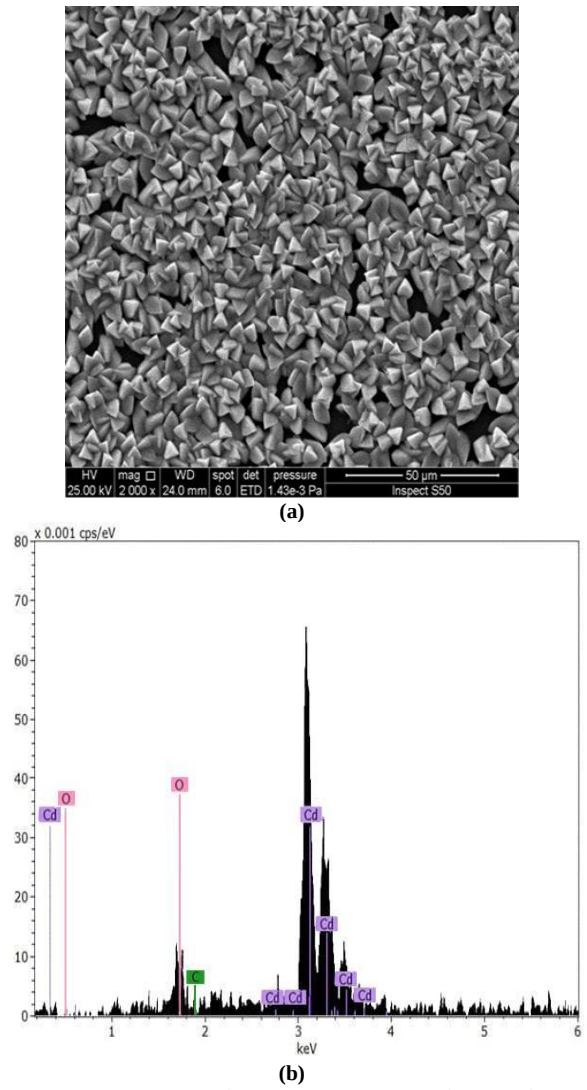

Fig. (2) SEM analysis of (a) image and (b) EDS for CdO films

4. Conclusion

CBD method was a suitable technique for a thin film deposition with low costing. The completing of stander conditions for CdO films could be supporting the progress and developing of heterojunction applications. The cubic crystalline of films identified the material and morphology. The optical properties had shown a good exhibit especially at visible wavelength region. Furthermore, the conductivity as a function with absolute temperature of oxide semiconductor CdO was revealed a great

ability for photodetector applications. In the concluded, the spectral responsively of photodetector CdO/ Si demonstrated that CdO has the unique properties for wide applications in heterojunction field. It is the road for our work progress on this material for future applications.

References

[1] 1. A. Mandeles, C.C., *Chemistry and Technology of Solid State Gas Sensor Devices.* Wiley & Sons Inc, New York, 1993.

[2] 2. Sharma, A.K., et al., *Nanostructured CdO–ZnO composite thin films for sensing application.* Journal of Materials Science: Materials in Electronics, 2020. **31**(23): p. 20932-20944.

[3] 3. A.D.A. Buba, D.O.S., *Synthesis and Characterization of Cadmium Oxide (Cdo) Deposited by Chemical Bath Deposition Technique.* International Journal of Current Research and Academic Review, September-2015. **3**.

[4] 4. Liu, H., et al., *ZnO Hierarchical Nanostructure Photoanode in a CdS Quantum Dot-Sensitized Solar Cell.* PloS one, 2015. **10**(9): p. e0138298-e0138298.

[5] 5. Ricardo Vidal Lorbada, T.W., David Fuertes Marrón, Tetiana Lavrenko and Dennis Muecke *A Deep Insight into the Electronic Properties of CIGS Modules with Monolithic Interconnects Based on 2D Simulations with TCAD.* Coatings, 2019. **9, 128**.

[6] 6. Naif Mohammed Al-Hada, H.M.K., Che Azurahanim Che Abdullah, Elias Saion, Abdul H Shaari, Zainal Abidin Talib, Khamirul Amin Matori, *Down-top nanofabrication of binary (CdO)x (ZnO)1–x nanoparticles and their antibacterial activity.* International Journal of Nanomedicine, 2021. **37.237.134.11**.

[7] 7. Andres Galdámez-Martinez , G.S., Frank Güell, Paulina R. Martínez-Alanis and Ateet Dutt, *Photoluminescence of ZnO Nanowires: A Review.* Nanomaterials, 2020. **10, 857**.

[8] 8. Borysiewicz, M.A., *ZnO as a Functional Material, a Review.* Crystals, 2019. **9, 505**.

[9] 9. Ziaul Raza Khan, M.S.K., Mohammad Zulfequar , Mohd Shahid Khan, *Optical and Structural Properties of ZnO Thin Films Fabricated by Sol-Gel Method.* Materials Sciences and Applications, 2011. **2, 340-345**.

[10] 10. William Vallejo, C.D.-U.a.C.Q., *Optical and Structural Characterization of Cd-Free Buffer Layers Fabricated by Chemical Bath Deposition.* Coatings, 2021. **11, 897**.

[11] 11. Mouna Khiari, M.G., Michaël Lejeune, Florica Lazar and Aomar Hadjadj, *Preparation of Very Thin Zinc Oxide Films by Liquid Deposition Process: Review of Key Processing Parameters.* Coatings, 2022. **12, 65**.

[12] 12. Thambidurai, M.D., Cuong, *Structural, morphological and optical properties of CdO nanostructures synthesized by chemical bath deposition method.* Materials Letters, Elsevier B.V., 2018.

[13] 13. R.R. Mahdi, S.A.M., *Synthesis and Properties of Cadmium Oxide Thin Films Prepared By Simple Chemical Method.* Energy Procedia, 2019. **157**.

[14] 14. M.R. DAS, A.M., P. MITRA, *Structural, optical and electrical characterization of CBD synthesized CdO thin films: influence of deposition time.* Materials Science-Poland, 2017. **63**.

[15] 15. KATI, N., *Controlling of optical band gap of the CdO films by zinc oxide.* Materials Science-Poland, 2018. **37(1)**: p. 136-141.

[16] 16. Ezekoye, B.A., Ezekoye, V.A., Offor, P.O., Utazi,, *Synthesis, structural and optical characterization of cadmium oxide (CdO) thin films by Chemical Bath Deposition (CBD) technique.* Inter. J. Phys. Sci., 2013. **8(3)**: p. 1597–1601.

[17] 17. Lalithambika, K.C., Shanthakumari, K., Sriram,, *Optical properties of CdO thin films deposited by chemical bath method.* Int. J. Chem. Tech. Res., 2014. **6(5)**: p. 3071–3077.

[18] 18. R. Kumaravel, S.M., S. Regina, M. Snegaa, and K. Ramamurthia, *Electrical,optical and structural properties of Aluminum doped Cadmium oxide thin films prepared by spray pyrolysis technique.* Materials Chemistry and Physics, 2010. **122**: p. 444–448.

Doping of Cadmium Oxide with Chromium by Laser-Produced Plasma

Basil S. Ahmed[1], Sabri J. Mohammad[1], Ghuson H. Mohammed[2]

[1] Department of Physics, College of Education for Pure Sciences, Tikrit University, IRAQ
[2] Department of Physics, College of Science, University of Baghdad, Baghdad, IRAQ

Abstract
In this work, laser-produced plasma at different energies (300, 400, 500, and 600 mJ) was used for doping cadmium oxide nanoparticles with chromium. These nanoparticles were coated on glass surfaces in thin layers (at a rate of 100 drops). The UV-visible spectrophotometer and x-ray diffraction (XRD) were used to examine it structurally and optically. With increasing laser intensities, the energy gap in the films changed from (1.8 eV) to (2.4 eV).

Keywords: Cadmium oxide; Pulsed-laser deposition; Nanomaterials; Structural properties
Received: 15 July 2020; **Revised:** 18 September 2020; **Accepted:** 1 October 2020; **Published:** 1 July 2021

1. Introduction

Cadmium oxide has a low electrical resistance because cadmium atoms are present at interstitial sites or via oxygen gaps. Cadmium oxide has a high absorption coefficient, allowing it to be used in solar systems to boost photovoltaic cell efficiency [1, 2]. Cadmium oxide is a semiconductor that belongs to the periodic table group (II-VI) [3], and it has a cubic crystal structure (Cubic) and a face-centered (f.c.c.) unit cell, which is comparable to the structure of a crystal of sodium chloride (NaCl) [4,5]. Cadmium oxide is a semiconductor material that belongs to the transparent conductive oxides (TCO) family [6-8]. It possesses peculiar features, such as a rather significant energy gap spanning between 1.8 and 2.4 eV [9] and apparent transparency. Near infrared rays (NIR) and the red region of the electromagnetic spectrum have high reflectivity [10], high carrier mobility [11], and high electrical conductivity similar to that of negative-type metals (n-type) [4,9], as well as good fluorescence and many applications in electro-optical devices, and display devices [12]. Cadmium oxide is one of the cadmium compounds that is soluble in acids and ammonia salts but insoluble in water or alkalis [13]. Cr^{+3} is not considered a health concern. Hexavalent chromium Cr^{+6} complexes are very poisonous and are typically formed by naturally occurring chromium(III) oxidation; they have a broad variety of industrial applications [14]. Transition metal oxide nanoparticles, in general, include a vast range of materials that have garnered substantial attention owing to their numerous catalytic, pharmacological, electrical, magnetic, and thermal properties. Chromium is a heavy metal that is widely used in electroplating, textile dyeing, pigmentation, and paper manufacturing [15]. Antimicrobial drugs, optical sensors, biomarkers, and drug delivery systems are just a few of the applications for nanoscale materials [16]. Nanoparticles, in comparison to bulk material, have a multifunctional feature due to their enormous surface ratio to volume area. The most important feature of the nanotechnology approach is the discovery of an efficient way of producing nanoparticles. Hydrothermal techniques [17], micro-emulsion [18], microwave irradiation [19], gelation [20], sol-gel [21], precipitation [14], combustion [22], and other methods have been documented for creating chromium nanoparticles.

2. Preparation Method

The target was prepared in powder form, and it was pressed into a disc with a diameter of 1cm and a thickness of 0.5cm, with a pressure of 6 Tons and a period of 20 min, then chromium-doped cadmium oxide (Cr-doped CdO) nanoparticles were prepared by

laser-induced plasma using an Nd:YAG laser (1064nm) with different energies (300, 400, 500 and 600 mJ). These nanoparticles were deposited in thin layers on glass surfaces using Cr-doped CdO (at a rate of 100 points), The UV-visible spectrophotometer, and the X-ray diffraction (XRD) were then used to examine them, and the findings indicated that the grain size and average roughness increase with increasing laser intensity. The optical characteristics of all films were also investigated, and the findings revealed that the absorption coefficient in the wavelength range 310-1000 nm was lowered by increasing laser energy within the range 1.8-2.7 eV.

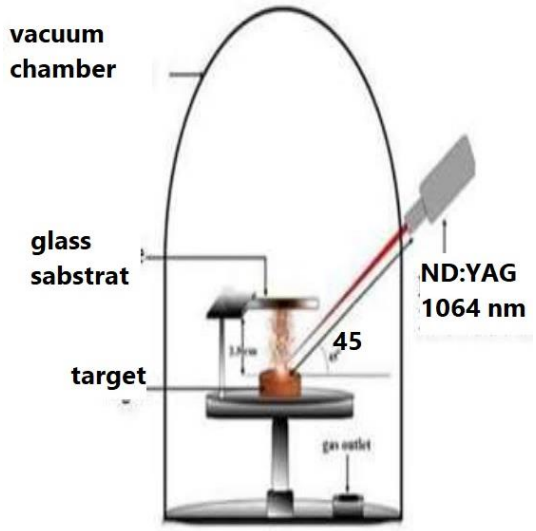

Fig. (1) Schematic diagram of the PLD system used in this work

The crystalline structure and grain size of the Cr-doped CdO films prepared using PLD technique were calculated using XRD. Scherrer's equation was used to compute the crystallite size (D) as [23]

$$D\ (Å) = k\lambda/\beta\cos\theta \quad (1)$$

where k is the Scherrer's constant (=0.9), λ is the x-ray wavelength (1.540Å), and β is the full-width at half maximum (FWHM) of the peaks at the θ diffraction angle from the Bragg's angle location

A double-beam Metertech SP8001 UV-Visible spectrophotometer was used to investigate the optical characteristics. The optical band gap was visually approximated using Tauc's equation for direct transition

$$ah\upsilon = K(h\upsilon - E_g)^n \quad (2)$$

where α is the absorption coefficient, K is proportionality constant, hυ is energy of the incident photon, and E_g is band gap energy, and n=0.5 for indirect band gap and n=2 for direct band gap

3. Results and Discussion

The x-ray diffraction method revealed that all of the thin films were made with a polycrystalline structure. The XRD patterns of the Cr-doped CdO composite films with varied energies are shown in Fig. (2).

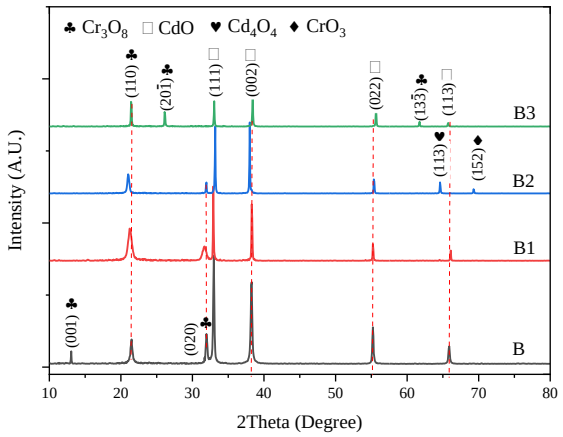

Fig. (2) The XRD patterns of samples prepared by PLD using different energies (B1=300mJ, B2=400mJ, B3=500mJ, B4=600mJ)

These patterns include peaks centered at 2θ of 13.05°, 21.48°, 26.36°, 31.99°, 32.97°, 38.28°, 55.22°, 61.66°, 65.87° and 66.05°, corresponding to Miller indices (001), (110), (20-1), (020), (11-3) and (152), respectively. The angles 13.05°, 21.48°, 26.36°, 31.99°, 61.66° and 66.05° belong to Cr. These findings coincide with ICSD card no. 98-015-5848, but not with Miller indices (111), (002), (022), (020) and (113). The angles 32.97°, 38.28°, 55.22° and 65.87 pertain to CdO. These findings are consistent with ICSD card no. 98-006-1554. The figure clearly shows that the Cr-doped CdO thin film has a polycrystalline structure and is preferentially oriented along (111) crystallographic orientation. It was observed that when the energy was 400mJ, the intensities of the peaks raised in a different manner for certain peaks, but when the energy was raised to 500 and 600 mJ, the intensities of the peaks decreased. Chromium and chromium oxide compounds

are generally monoclinic crystal systems, while CdO has a cubic crystal system. The film may be observed to be orientated preferentially along (111) crystallographic orientation as well as (022), (002) and (003). (113). This reflects the uniformity of the film material and the relative purity of the target employed, whereas several peaks emerged when the energies were raised. This is due to increased evaporation rates and corresponds with [24].

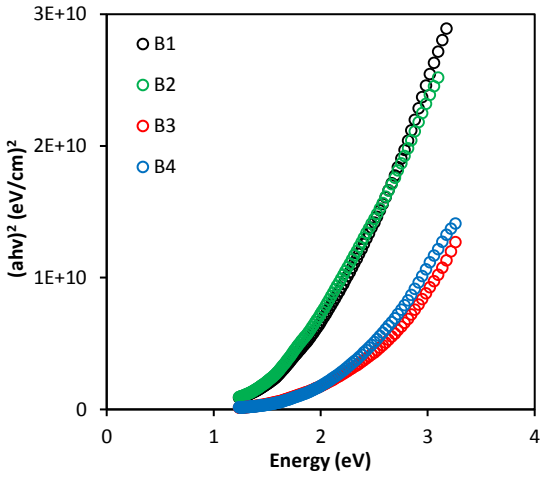

Fig. (7) determination of energy band gap for the samples prepared in this work

The optical energy gap of allowed direct electronic transitions in Cr-doped CdO thin films was calculated using Tauc's equation (Eq. 2) [22] as the value of *n* is 0.5 by drawing a straight line between $(ahv)^2$ and the incident photon energy (hv) and extending the straight line to intercept the photon energy axis at the point $(ahv)^2=0$. The optical energy gap for direct transport of Cr-doped CdO films is shown in Fig. (7). It is found that the value of the energy gap decreases as laser energy rises, resulting in the creation of localised levels in the conduction band, and hence photon absorption increases as laser energy increases as shown in Fig. (8). The values are reported in Table (3). These findings are found to be consistent with [23].

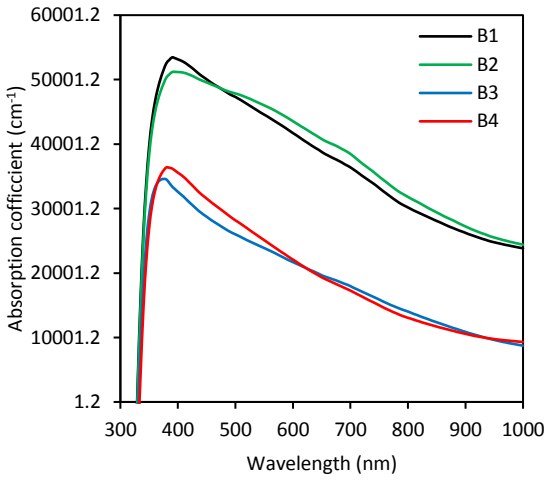

(b)

Fig. (8) Variation of absorption coefficient of the prepared samples with wavelength

4. Conclusions

Pulsed-laser deposition (PLD) was used to deposit the Cr-doped CdO thin films on glass substrates. According to the XRD, all thin films were polycrystalline and had a cubic structure for CdO compounds with the (111) orientation being prevalent. It demonstrated control (110) for (Cr) compounds, and the AFM findings revealed a rise in the average diameters and average thicknesses of the deposited films with increasing laser power. In terms of optical property measurements, it was discovered that the absorption coefficient rose as laser power increased. On the other hand, the energy gap increases with an increase in laser energy with a slight variation in the values, indicating that the effect of energies is somewhat close, while FE-SEM examinations revealed the presence of nanoclusters with an increase in diameter and particle size as energies increased.

References

[1] R.K. Gupta et al., "Wide band gap $Cd_{0.83}Mg_{0.15}Al_{0.02}O$ thin films by pulsed laser deposition", *Appl. Surf. Sci.*, 255 (2009) 4466-4469.

[2] Z. Zhao, D.L. Morel and C.S. Ferekides, "Electrical and optical properties of tin-doped CdO films deposited by atmospheric metalorganic chemical vapor deposition", *Thin Solid Films*, 413 (2002) 203-211.

[3] C.H. Bhosale et al., "Structural, optical and electrical properties of chemically sprayed CdO thin films", *Mater. Sci. Eng. B*, 122 (2005) 67-71.

[4] T. Ghoshal, S. Kar and S. Chaudhuri, "Synthesis of nano and micro crystals of $Cd(OH)_2$ and CdO in the shape of hexagonal sheets and rods", *Appl. Surf. Sci.*, 253 (2007) 7578-7584.

[5] A.A. Dakhela and A.Y. Ali-Mohamed, "Structural, electrical, and optical absorption properties of $La_xCd_{1-x}O$ solid solution films obtained by sol–gel method", *Mater. Chem. Phys.*, 113 (2009) 356-360.
[6] S. Ilican et al., "CdO:Al films deposited by sol–gel process: a study on their structural and optical properties", *Optoelectron. Adv. Mater. - Rapid Commun.*, 3(2) (2009) 135-140.
[7] D.M. Carballeda-Galicia et al., "", *Thin Solid Films*, 105 (2000) 371.
[8] Y. Caglar, S. Ilican and M. Caglar, "Single-oscillator model and determination of optical constants of spray pyrolyzed amorphous SnO_2 thin films", *Euro. Phys. B*, 58(3) (2007) 251-256.
[9] A.A. Dakhel, "Influence of hydrogenation on the electrical and optical properties of CdO:Tl thin films", *Thin Solid Films*, 517 (2008) 886-890.
[10] Y. Zhang and J. Mu, "Preparation of CdO Thin Films by Annealing Cd^{+2}-Dithiol Self-Assembled Films", *Disper. Sci. Technol.*, 26 (2005) 509-511.
[11] X. Li et al., "High Mobility CdO Films and Their Dependence on Structure", *Electrochem. Solid-State Lett.*, 4 (2001) 66-68.
[12] A.A. Dakhel and A.Y. Ali-Mohamed, "Structural and optoelectrical properties of nanocrystalline Gd-doped CdO films prepared by sol gel method, *Sol-Gel Sci. Technol.*, 55 (2010) 348-353.
[13] P. Pradyot, **"Handbook of Inorganic Chemicals"**, McGraw-Hill, Inc., (NJ, 2003) 152.
[14] W.T. Cefalu and F.B. Hu, "Role of Chromium in Human Health and in Diabetes", *Am. Diabetes Assoc.*, 27(11) (2004) 2741-2751.
[15] C. Sukumar et al., "Significance of co-immobilized activated carbon and Bacillus subtilis on removal of Cr(VI) from aqueous solutions", *Environ. Earth Sci.*, 72(3) (2014) 839-847.
[16] D. Bhattacharya and R. Gupta, "Nanotechnology and potential of microorganisms", *Crit. Rev. Biotechnol.*, 25(4) (2005) 199-204.
[17] L. Sheng et al., "Highly sensitive room-temperature gas sensors based on hydrothermal synthesis of Cr_2O_3 hollow nanospheres", *Chinese Phys. B*, 18(9) (2009) 3985-3989.
[18] R. Karimian, F. Pirib, and S.J. Davarpanaha, "Synthesis of zinc oxide and chromium (III) oxide nanoparticles with diverse physiological properties", *J. Appl. Biotechnol. Rep.*, 1(2) (2014) 73-76.
[19] F. Farzaneh and M. Najafi, "Synthesis and Characterization of Cr_2O_3 Nanoparticles with Triethanolamine in Water under Microwave Irradiation", *Iran J. Sci.*, 22(4) (2011) 329-333.
[20] D.W. Kim et al., "Preparation of chromia nanoparticles by precipitation-gelation reaction", *Mater. Lett.*, 58(12-13) (2004) 1894-1898.
[21] S.M. El-Sheikh, R.M. Mohamed and O.A. Fouad, "Synthesis and structure screening of nanostructured chromium oxide powders", *J. Alloys Compd.*, 482(1-2) (2009) 302-307.
[22] X.-Z. Fu et al., "Ethane dehydrogenation over nano-Cr_2O_3 anode catalyst in proton ceramic fuel cell reactors to co-produce ethylene and electricity", *J. Power Sources*, 196(3) (2011) 1036-1041.
[23] S.M. Hanfoosh and N.K. Hassan, "Optical Properties of Mixed ZnO:Fe_2O_3 Grown via Pulsed laser deposition", *Iraqi J. Sci.*, 60(9) (2019) 2009-2014.
[24] K.A. Aadim and M.M. Shehab, "Influence of Laser Energy on the Structural and Optical Properties of (CdO):(CoO) Thin Films Produced by Laser-Induced Plasma (LIP)", *Iraqi J. Phys.*, 19(49) (2021) 42-45.

Table (1) Results obtained by XRD measurements performed on samples with different energies

Energy (mJ)	Material	Exp. 2θ (deg)	FWHM Left [deg]	hkl	G.S (nm)	Crystal system	Reference code
300	Cr	13.05	0.096	0 0 1	90.8	Monoclinic	ICSD 98-015-5848
		21.48	0.31	1 1 0	26.8	Monoclinic	ICSD 98-015-5848
		31.99	0.241	0 2 0	35.5	Monoclinic	ICSD 98-015-5848
	CdO	32.978	0.183	1 1 1	47.2	Cubic	ICSD 98-006-1554
		38.249	0.227	0 0 2	38.4	Cubic	ICSD 98-006-1554
		55.22	0.197	0 2 2	47.6	Cubic	ICSD 98-006-1554
		65.87	0.222	1 1 3	35	Cubic	ICSD 98-006-1554
400	Cr	21.2716	0.1443	1 1 0	59.4	Monoclinic	ICSD 98-015-5848
		31.6627	0.2346	0 2 0	36.4	Monoclinic	ICSD 98-015-5848
	CdO	32.982	0.3819	1 1 1	22.2	Cubic	ICSD 98-006-1554
		38.3117	0.3019	0 0 2	28.6	Cubic	ICSD 98-006-1554
		55.2744	0.4236	0 2 2	21.6	Cubic	ICSD 98-006-1554
		66.0561	0.3388	1 1 3	28.6	Cubic	ICSD 98-006-1554
500	Cr	21.2412	0.3035	1 1 0	27.4	Monoclinic	ICSD 98-015-5848
		31.6892	0.2168	0 2 0	39.5	Monoclinic	ICSD 98-015-5848
	CdO	32.9923	0.2838	1 1 1	30	Cubic	ICSD 98-006-1554
		38.2764	0.2064	0 0 2	42.5	Cubic	ICSD 98-006-1554
		55.2834	0.1806	0 2 2	51.8	Cubic	ICSD 98-006-1554
		66.0452	0.1806	1 1 3	54.8	Cubic	COD 96-900-6677
	Cr	69.1457	0.2838	1 5 2	35	Orthorhombic	ICDD 00-001-0622
600	Cr	21.7006	0.09	1 1 0	98.6	Monoclinic	ICSD 98-015-5848
		26.3638	0.3054	2 0 -1	27.4	Monoclinic	ICSD 98-015-5848
	CdO	33.0882	0.2763	1 1 1	30.9	Cubic	ICSD 98-006-1554
		38.3173	0.2618	0 0 2	33.1	Cubic	ICSD 98-006-1554
		55.2992	0.2618	0 2 2	35.3	Cubic	ICSD 98-006-1554
	Cr	61.6671	0.32	1 3 -3	29.7	Monoclinic	ICSD 98-015-5848
	CdO	65.8664	0.2618	1 1 3	37.3	Cubic	ICSD 98-006-1554

Characterization and Antimicrobial Activity of Copper Oxide Nanoparticles

Thaer A. Mezher[1], Abdullah M. Ali[1], Ahmed N. Abd[2]

[1] Department of Physics, College of Education for Pure Sciences, Tikrit University, IRAQ
[2] Department of Physics, College of Science, Mustansiriyah University, Baghdad, IRAQ

Abstract
Researchers are interested in green technology because it is a low-risk, eco-friendly, and affordable way to biosynthesize nano-particles. Copper nitrate trihydrate and Nigella sativa extract were used as a reducing and capping agent during the manufacture of copper oxide (CuO) NPs in this investigation.. The biosynthesized CuO NPs were characterized using X-ray diffractometer transmission electron microscopy و UV-Vis spectroscopy, Scanning Electron Microscopy and Fourier transform infrared spectroscopy (FTIR). Good crystalline nature which perfectly matches the monoclinic structure of bulk CuO. The results obtained from TEM also showed that CuO NPs were semi spherical in shape, while the Zeta potential characterization indicated that the prepared particles have low stability. Moreover, CuO NPs showed good antimicrobial activity.

Keywords: Green synthesis; Nigella Sativa; Copper oxide; Nanoparticles; Antibacterial activity
Received: 8 May 2020; **Revised:** 22 August 2020; **Accepted:** 29 August 2020; **Published:** 1 July 2021

1. Introduction

Materials exhibiting distinctive characteristics when compared to bulk materials are known as nanoparticles (NPs), which range in size from 1 to 100 nm [1]. Their higher surface area/volume ratio is an important distinguishing feature that allows them to work in a range of industries, including the chemical, food, electrical, and healthcare industries [2-3]. Recently, the discovery of metal and metal oxide NPs has substantially benefited the biomedical field in terms of biosensing, imaging, diagnosis, and treatment [4-5]. The three metals and their oxides that are used the most frequently are gold (Au), silver (Ag), and copper (Cu). Cu, which is less expensive than Au and Ag, is the most cost-effective of them all [6]. CuO and Cu_2O are the two principal copper oxide phases. Both are p-type semiconductors. Bulk CuO has a bandgap of 1.2-1.9 eV, whereas bulk Cu_2O has a bandgap of 1.8-2.5 eV. Because of their electrical and optical characteristics, as well as their nontoxicity, natural abundance, and low cost, they are potential semiconductors for a wide range of applications [7]. Copper oxide nanoparticles were created using a variety of physical and chemical processes. It involved the use of toxic chemicals that are hazardous to persons and the environment, as well as the requirement for a lengthy period of time, high expenditures, and significant energy depletion. In addition, the resulting nanomaterials are unstable and agglomerate quickly unless proven agents are added to them, as well as liberate toxic and dangerous by-products to the environment, so it was found necessary The trend toward simple methods in the preparation of nanomaterials, such as the green method of preparation that called “green synthesis”, which is characterized as being environmentally friendly, that is, less harmful to the ecosystem and at low costs, and focuses on producing the required material quickly without the presence of harmful by-products to the environment, as well as with purity and high quality of the oxide prepared with it. The role of the plant extract in the method and also enjoying the preparation is the reduction of salt to nano-metal oxide. [8-9].

Our current study includes the preparation of copper oxide nanoparticles by green synthesis using black seed extract and application of the product in the medical field

to be used as an inhibitor of bacterial activity.

2. Experimental Work

CuO NPs were prepared by green synthesis technology of high purity Copper (III) nitrate trihydrate (99.5%, $Cu(NO_3)_2.3H_2O$) provided by (General Drug House, India) in distilled water (DW) at room temperature (RT) with a reducing agent consisting of Nigella sativa seed extract. The preparation process goes through two stages: the stage of preparing the plant extract and the stage of preparing the nanomaterial. For the first stage, the seeds of Nigella sativa are cleaned well by water, dried, and then milling into fine particles using a laboratory grinder. A 1g of finely milling seeds particles is dissolved in (100) ml of distilled water in a 150 flat-bottom beaker. It was heated with a hotplate magnetic stirrer at 50°C for half an hour. The aqueous extract was filtered using filter paper. A 2.41g of $Cu(NO_3)_2.3H_2O$ was added to 100ml of distilled water. For one hour, the mixture is heated on a hot plate with a magnetic stirrer until the nitrate is completely dissolved. A 5ml of plant extract solution is then added, gradually and at the same temperature, to the mixture to create an aqueous solution. The hue of the solution gradually changes to green. The production of nanoparticles is shown by the progressive change in colloidal color, as seen in Fig. (1).

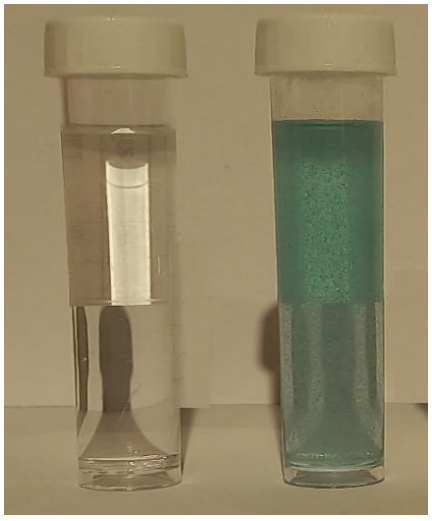

Fig. (1) Distilled water (left) and CuO NPs colloidal induced by green synthesis (right)

The colloidal CuO nanoparticles were deposited on glass substrate by using drop casting technique at 60°C as shown in Fig. (2). Structural, morphological and optical properties of CuO NPs were investigated by XRD 2700AB diffractometer (HAOYUAN, Zhejiang, China), scanning electron microscopy (MIRA3-FRENCH, SEM), and transmission electron microscopy (Philips em 208s 100kV TEM).

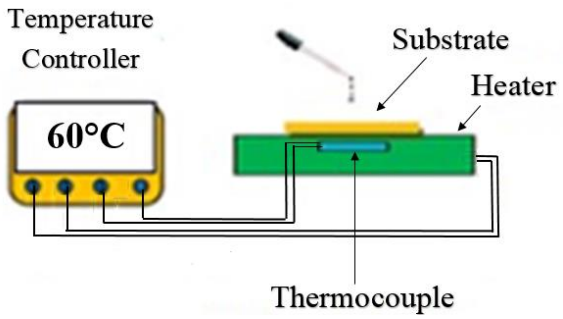

Fig. (2) Drop casting technique to precipitate the solution on a glass substrate

3. Results and Discussion

The crystal phases and crystallite size of nanoparticles were confirmed by XRD. An x-ray diffractometer with Cu-K crystal radiation (1.54Å) scanning at a rate of (5°/min) over a (2θ) range of 20°-80° was used for the study. Diffraction peaks were detected by comparing experimental and standard 2 values. Figure (3) depicts the XRD pattern of a CuO layer produced via green synthesis and placed on a glass substrate. From the above figure, we can notice the presence of a first peak at 23.53° and a second peak at the angle 28.10° indicating copper oxide according to the international standard JCPDS card no. 89-5895 as shown in table (1), as it agrees to a certain extent with the results of reference [10]. The FWHM is the full-width at half maximum of the XRD pattern was used to determine the average crystallite size (D_{av}) by Scherrer's equation [11]:

$$D_{av} = k\lambda/\beta \cos \theta_B \quad (1)$$

The micro-strain (η), and the dislocation density (δ) was calculated by the following two equations [12]:

$$\delta = 1/ (D_{av})^2 \quad (2)$$

$$\eta = \beta \cot \theta / 4 \quad (3)$$

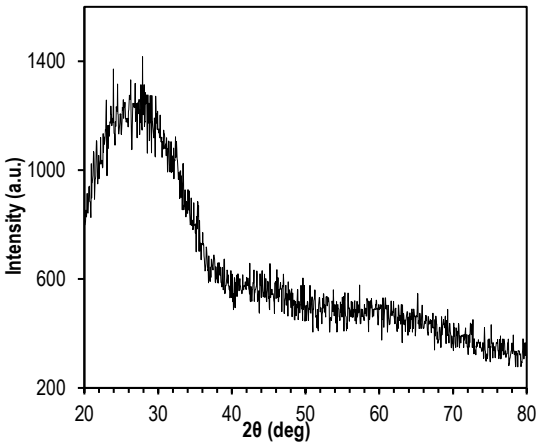

Fig. (3) XRD pattern of CuO film prepared in this work

Table (1) Structural parameters calculated from XRD pattern of (CuO) film

$2\theta_{std}$ (deg)	$2\theta_{exp}$ (deg)	FWHM (deg.)	d-space (Å)	D_{ave} (nm)	$\delta \times 10^{-4}$ $(nm)^{-2}$	$\varepsilon \times 10^{-4}$
23.53	23.94	0.048	7.58	2.95	117.36	1145.25
28.10	27.89	0.045	6.32	3.17	109.15	992.29

XRD analysis supports the production of CuO nanoparticles. The broad peaks in XRD pattern indicated that the average particle size of the CuO nanoparticles is close to 100 nm, which was confirmed by TEM results.

Figure (4) shows a FE-SEM image of copper oxide nanoparticles manufactured by green synthesis method and deposited on glass substrate. This image of a CuO sample with a resolution of 1 µm and 200 nm, shows that the prepared nanoparticles have an oval shape that is very similar to the shape of a wheat grain, close to each other and with particle size of about 35.11 nm. The nanoparticles agglomerate together to form a shape very similar to the shape of a flower.

The shape and size of the prepared particles were illustrated with the help of TEM (Fig. 5). The results of TEM showed a group of distinct spherical and semispherical nanoparticles of two types, where the first group is called large structures whose dimensions exceed 40-60 nm, and they are particles that contain proteins within their structure, which is a special characteristic of the green plant synthesis method, and this was also confirmed by FTIR. These protein substances can also act as containment and stabilizing agent. As for the second group, which represents CuO nanoparticles, which have dimensions smaller than the values of the first group, ranging between 20-40 nm, which is distinguished by a dark black color.

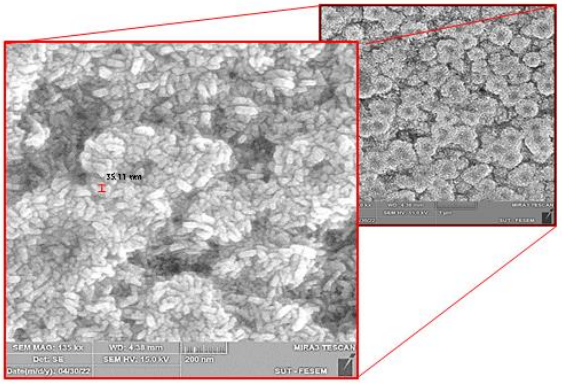

Fig. (4) FE-SEM image of CuO NPs prepared in this work

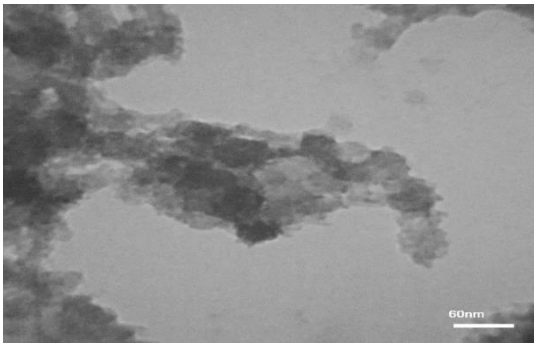

Fig. (5) TEM image of CuO NPs prepared in this work

The results also indicate that the presence of proteins leads to reducing the zeta potential to low values due to the occurrence of the accumulation phenomenon as observed in the FE-SEM result.

The agar well diffusion method was used to evaluate synthetic CuO NPs for antibacterial and antifungal activity against pathogens (Gram +ve and Gram -ve bacteria).

The biological activity of four different types of bacteria (E. coli, Klebsiella spp., S. aureus, S. epidermidis) is depicted in Fig. (6) under the effect of the prepared nanoparticles and a clear inhibitory diameter was given by table (2).

Nanoparticles disrupt proteins and enzymes, destabilize the ribosome, interfere with mitochondrial processes, and reside in the electron transport chain when they enter the cell. Additionally, these nanoparticles actively obstruct DNA-like transcriptional

processes and cause cell death by obstructing cell division and the respiratory chain. On the other hand, the amount of adsorption by Candida fungi to copper oxide nanoparticles prepared by green synthesis was measured, as it was found that the absorption of this fungus was 31 mm as shown in Fig. (7).

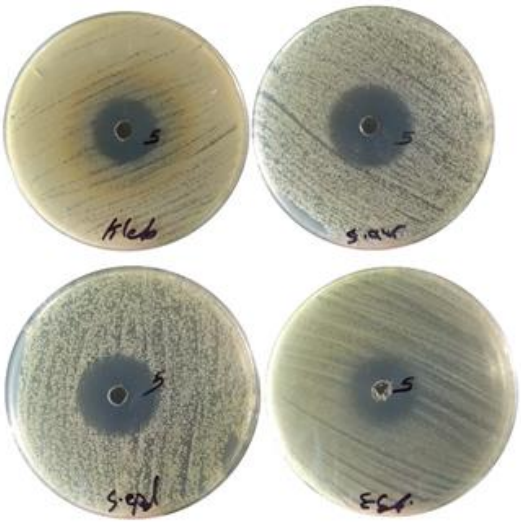

Fig. (6) Biological activity of different types of bacteria

Table (2) The inhibition zone of CuO NPs by bacteria

Bacteria	Inhibition zone (mm)
S.aureus	28
S.epidermidis	27
E.coli	20
Klebseilla spp	22

Fig. (7) Iinhibition zone of CuO NPs absorbed by fungi

4. Conclusions

The current study showed that Nigella Sativa seed is one of the renewable sources for preparing copper oxide nanoparticles in a safe, fast, simple and cheap way. The particles were also diagnosed using different techniques such as the FTIR, which proved that they were in the range 600-700 cm^{-1}. The particles also showed good activity in inhibiting bacteria and fungi species, which depend largely on the size and shape of the particles and the method of preparation used.

References

[1] C. Riggio et al., "Nano-oncology: clinical application for cancer therapy and future perspectives", *J. Nanomater.*, 2011 (2011).
[2] C. Contado, "Nanomaterials in consumer products: a challenging analytical problem", *Front. in Chem.*, 348 (2015).
[3] S. Ibrahim et al., "Nanowires nickel oxide and nanospherical manganese oxide synthesized via low temperature hydrothermal technique for hydrogen peroxide sensor", *J. Chem.*, 2016 (2016).
[4] Y. Wang et al., "Cuprous oxide nanoparticles inhibit prostate cancer by attenuating the stemness of cancer cells via inhibition of the Wnt signaling pathway", *Int. J. Nanomed.*, 12 (2017) 2569.
[5] A.I. Jeffree et al., "Biosensors approach for lung cancer diagnosis—a review", *RITA*, 2018 (2020) 425-435.
[6] B. Jia et al., "Preparation of copper nanoparticles coated cellulose films with antibacterial properties through one-step reduction", *ACS Appl. Mater. Interfaces*, 4(6) (2012) 2897-2902.
[7] M.H. Oudah et al., "Synthesis of copper oxide thin films by electrolysis method based on Porous Silicon for Solar Cell Applications", *IOP Conf. Ser.: Mater. Sci. Eng.*, 757(1) (2020).
[8] P.C. Nagajyothi et al., "Green synthesis: in-vitro anticancer activity of copper oxide nanoparticles against human cervical carcinoma cells", *Arab. J. Chem.*, 10(2) (2017) 215-225.
[9] K. Nithya et al., "Preparation and characterization of copper oxide nanoparticles", *Int. J. Chem. Tech. Res.*, 6(3) (2014) 2220-2222.
[10] A.B. Shinde, D.A. Mhamane and S.V. Nishandar, "Experimental investigation of rheological properties of water lubricant by adding CuO nano particles", *AIP Conf. Proc.*, 2200(1) (2019).
[11] R.D.A Jalill, R.S. Nuaman and A.N. Abd, "Biological synthesis of titanium dioxide nanoparticles by curcuma longa plant extract and study its biological properties", *World Sci. News*, 49(2) (2016) 204-222.
[12] A.N. Abd, M.F. Al-Marjani and Z.A. Kadham, "Antibacterial activity of cadmium oxide nanoparticles synthesized by chemical method", *J. Multidiscip. Eng. Sci. Technol.*, 3(6) (2016) 5007-5011.
[13] H. Veisi, S. Hemmati and H. Javaheri, "N-Arylation of indole and aniline by a green synthesized CuO nanoparticles mediated by Thymbra spicata leaves extract as a recyclable and heterogeneous nanocatalyst", *Tetrahedron Lett.*, 58(32) (2017) 3155-3159.

Characterization and Parameters of Indian Costus Plasma Produced by Q-Switched Nd:YAG Laser

Hadder M. Abdullah, Alyaa H. Ali

Department of Physics, College of Science for Women, University of Baghdad, Baghdad, IRAQ

Abstract

The Indian costus plasma properties are investigated including electron temperature electron density, plasma frequency, Debye sphere length, and Debye number, using the spectrum of optical emission technique over energy range of 300 to 600 mJ. The Boltzmann plot is used to calculate the temperature, whereas Stark's line broadening is used to calculate the electron density. The Indian costus was spectroscopically examined in the air with the laser at 10 cm away from the target and the optical fiber at 0.5 cm away. The results were obtained for an electron temperature range of 1.8-2.2 eV and a wavelength range of 300-600nm. The XRF analysis reveals that the Indian costus contains a variety of minerals, each with a different percentage, which explains why the optical emission spectrum has so many peaks. When the laser energy lies between 300 and 600 mJ, the optical emission spectroscopy (OES) has been used to analyze the plasma spectrum of the Indian costus in the air. The results shows that as the laser energy grew, the Debye number will be greater (Nd) >>>1, which is one of the plasma properties.

Keywords: Optical emission spetrometry; Boltzmann plot; Stark's broadening; Pulsed-laser deposition
Received: 1 July 2020; **Revised:** 15 November 2020; **Accepted:** 22 November 2020; **Published:** 1 July 2021

1. Introduction

One of the largest angiosperm families, Astreaceae has around 23,600 species of plants, including trees, shrubs, and herbs in 1,620 genera. There are roughly 300 species in the Saussure genus [1]. Indian costus roots' chemical make-up has been studied since the 1950s. Many chemicals have been isolated up until this point. Although anthraquinones, alkaloids, and favonoids are also present, terpenes are the most active ones [2]. Due to its many benefits, laser-induced breakdown spectroscopy (LIBS) is becoming a more popular technique in atomic spectroscopy. A laser pulse is focused onto a sample using a high-powered laser, a mirror, and a lens in LIBS, which requires little to no sample preparation. It is possible to study solids, liquids, and gases using LIBS sampling that is initiated by optical absorption processes. [3]. The plasma is created when the energy from the laser pulse warms, ablates, atomizes, and ionizes the sample material. To resolve and detect the plasma's light, a spectrograph and a detector are used. The resulting plasma spectrum can be utilized to derive quantitative and qualitative information from the plasma, including its elemental composition. Information about plasma temperature and electron density can be gleaned from the widths, forms, and forms, and fluctuations of emission lines [4].

2. Material and Methods

The temperature of plasma represent the important parameter of thermodynamic because it can characterize and forecast other plasma aspects including relative populations of energy levels and particle speed distribution. The Boltzmann plot approach was used, which assumes that local thermodynamic equilibrium (LTE) has been attained within the plasma. According to estimates, LTE is usually achieved after a few hundred nanoseconds following plasma creation using LIBS with irradiances more than 108 W/cm^2 under normal air pressure 2.5×10^{-2}m bar. In the LIBS community, the plot of Boltzmann approach offers a more precise way of measuring plasma temperatures. The temperature (T), which represents the average temperature of the

plasma, has been obtained using the following equation [5]

$$T = \frac{(E_2 - E_1)}{k \ln(\frac{I_1 \lambda_1 A_2 g_2}{I_2 \lambda_2 A_1 g_1})} \quad (1)$$

where the intensity is I, the statistical weight is g, A is the probability of transformation, the wavelength is λ, E is the energy in eV of the excited state and k is the Boltzmann's constant

The density (n_e) can be calculated using the following equation [6]:

$$n_e = \frac{I_1}{I_2^*} 6.04 \times 10^{21} T^{\frac{3}{2}} e^{\frac{E_1 - E_2 - X_Z}{kT}} \quad (2)$$

where

$$I_2^* = \frac{I_2 \lambda_2}{g_2 A_2} \quad (3)$$

here, X_z denotes the organism's ionizing potential at ionizing level 2 Z in eV, I_2 denotes the line intensity for a transfer from top-level 2 to level 1, g_2 denotes the statistical move weight from level 2, A_2 denotes the transition eventuality from level 2 to level 1, and the subscript z denotes the species ionization stage for the referred species [7]

The plasma frequency is computed using the following equation [8]

$$f_p = 8.98\sqrt{n_e} \quad \text{(Hz)} \quad (4)$$

One of the most fundamental plasma features is frequency, which is purely reliant on plasma density. The plasma frequency is often very high due to the small size of ne [4]. Debye sphere length is the reaction of charged particles to limit the effect of local electrical fields, and it is this shielding that gives the plasma its quasi-neutrality property. The Debye sphere length is defined by [9,10]:

$$\lambda_D = \sqrt{\frac{\varepsilon_0 k_B T_e}{n_e e^2}} = 7.43 \times 10^2 \sqrt{T_e / n_e} \quad (5)$$

In compared to the machine's dimensions, Debye's length should be short. This first need is defined as follows for plasma life [11,12]:

$$\lambda_D <<< L \quad (6)$$

The device's length (in cm) is L, while its width (in cm) is Nd. Describing the density of particles on Debye's surface, in which $N_D >>> 1$ for the plasma condition [13]

$$N_D = (\frac{4\pi}{3}) n_e \lambda_D^3 \quad (7)$$

The tablets (pellets) were made from a 1.5 g sample of Indian costus plant, crushed by a piston at (six Pa) for ten minutes, and yielded granules with a diameter and thickness of 20 mm, according to the amount of material measured. The powdered Indian costus plant and the pressed Indian costus plant powder are shown in Fig. (2).

Fig. (2) The Indian Costus plant powder and its pellets

A 1064nm Nd:YAG laser with 6 Hz pulse repetition rate and various energies ranging from 300 to 600 mJ was used to study the emission spectrum of the Indian Costus specimen. The laser was positioned at 10 cm away from the sample. A lens with a shorter focal length, larger breakdown, and shallower focus depth can produce a small beam waist, as seen in Fig. (3). As for the LIBS, light emitted from the sample after being hit by the pulse laser was used to operate the spectrometer. The light emitted was examined in the setting using the short response time spectrometer optics. The optical fiber, was positioned at a roughly 45° angle as shown in Fig. (3). The spectrum analyzer detect the spectrum emitted from Indian Costus plasma within a spectral range of 300-600 nm [12].

3. Result and Discussion

Table (2) shows the laser energy and statistical coefficient (R), the best energy value that gives linear suitability is 600mJ, it gives value of 0.8542 which is closer to one, as the energy increase the suitability increase. Figure (6) shows the Stark distribution of the Indian Costus target at different laser energies. The intensity increased as the energy increased. Figure (7) shows the measured electron temperature (T_e) values using the Boltzmann plot which shows that as the laser

pulse energy is increased, the electron temperature (T_e) and the electron density (n_e) increase in air. At high laser powers, the duration of Debye (D) grows with increasing laser energy as shown in figures (8) and (9) because plasma frequency (f_p) are proportional to laser energy. The plasma frequency (f_p) increase because it is proportional to density (n_e). A plasma parameter energy (300-600mJ) are shown in table (3). These two parameters of Indian costus pellets increase with various laser energy. All plasma properties increase as the energy is increased according to the results.

Table (2) Laser energy and statistical coefficient (R^2)

Energy (mJ)	Statistical coefficient (R^2)
300	0.816
400	0.8303
500	0.846

Table (3) Plasma parameters for Indian costus with different laser energies in the air

Laser Energy (mJ)	FWHM (nm)	T_e (eV)	ne*10^{18} (cm-3)	fp x10^{13} (Hz)	λ_D x10^{-7} (cm)	N_D
300	2.83	1.86209223	3.03	1.56314	5.82463	2.506775
400	3.03	1.946256048	3.03	1.56314	5.9548	2.678635
500	3.21	2.115392211	3.21	1.6089	6.03159	2.948959
600	3.5	2.205687353	3.5	1.68	5.8983	3.006884

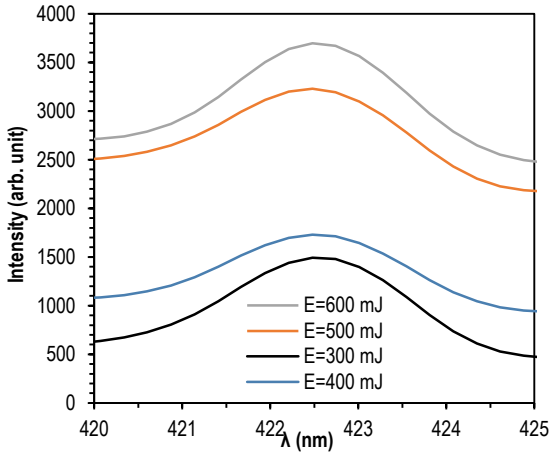

Fig. (6) The stark distribution of the Indian Costus target at different Laser Energies

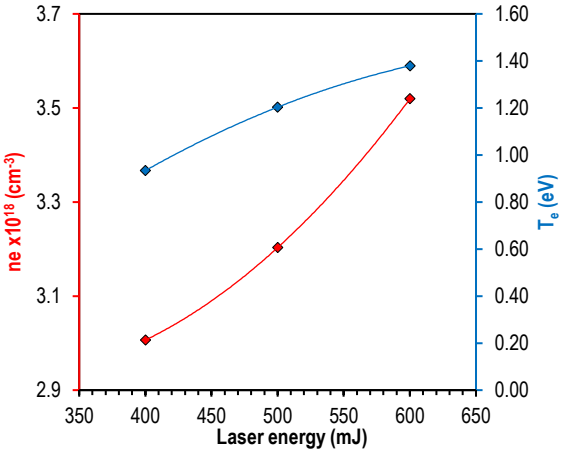

Fig. (7) Difference of (T_e) and (n_e) against laser energy of the Indian Costus target

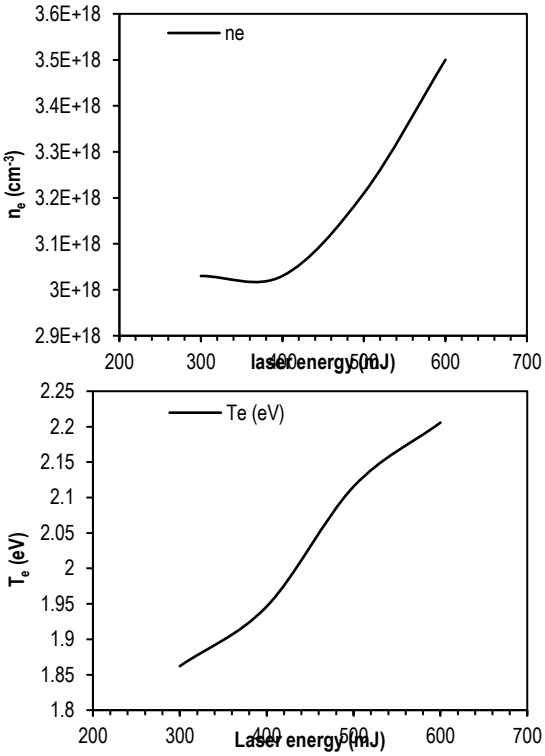

Fig. (8) Difference of (T_e) and (n_e) against laser energy of the Indian Costus target

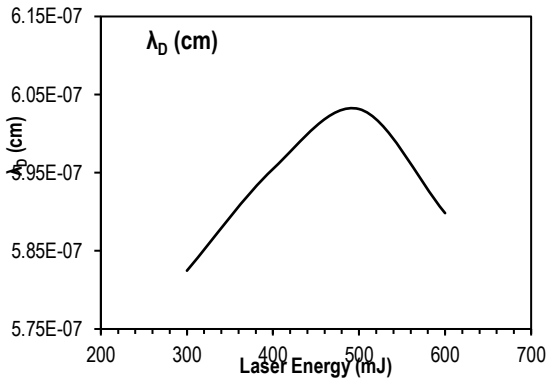

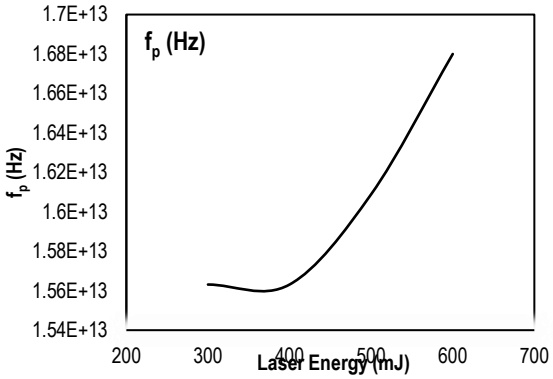

Fig. (9) Determination of Debye length (λ_D) and the plasma (f_p)

4. Conclusion

The Indian costus plasma parameters is created using the laser. Laser-plasma produces spectrum emission line that depend on the circumstances. It was founded that the laser intensities are influenced by the plasma parameter, an increasing in the laser's power causes an increase in the electron condensation in various laser atom forces, as well as an increase in Debye length, plasma frequency, and the number of Debye particles, it is also slight increase in the electron's temperature. The plasma characteristics for Indian costus with various laser energy grew as the energies increased. The energies were 300-600mJ because the research material is food, and the high energy will destroy the bonds that make up the substance, therefore, high energies has been not used. The plasma produced from the spectrum and this was investigated from the value of N_D where $N_D>>>1$.

References

[1] A. Ali et al., "Saussurea lappa An Important Medicinal Plant for Treatment Different Diseases: A review", *Kufa J. Nat. Sci.*, 11(1) (2021) 1–19.

[2] K. Zahara et al., "A review of therapeutic potential of Saussurea lappa-An endangered plant from Himalaya", *Asian Pac. J. Trop Med.*, 7 (2014) 60-69.

[3] R.C. Chinni, "Temperature and Electron Density Determination on Laser-Induced Breakdown Spectroscopy (LIBS) Plasmas", *Phys. Chem. Exp.*, 89(5) (2012) 678-680.

[4] D.W. Hahn and N. Omenetto, "Laser-induced breakdown spectroscopy (LIBS)", part II: review of instrumental and methodological approaches to material analysis and applications to different fields, *Appl. Spectro*., 66(4) (2012) 347-419.

[5] G.H. Jihad and K.A. Aadim, "Spectroscopic study the plasma parameters for Pb doped CuO prepared by pulse Nd:YAG laser deposition", *Iraqi J. Phys.*, 16 (2018) 1-9.

[6] A.D. Cremers, **"Handbook of Laser-Induced Breakdown Spectroscopy"**, 2nd ed., John Wiley & Sons (2013).

[7] H.A. Yuan et al., "Investigation of laser-induced plasma at varying pressure and laser focusing", *Spectrochimica Acta B: Atom. Spectro.*, 150 (2018) 33-37.

[8] K.A. Aadim et al., "Influence of Gas Flow Rate on Plasma Parameters Produced by a Plasma Jet and its Spectroscopic Diagnosis Using the OES Technique", *IOP Conf. Ser. Mater. Sci. Eng.*, 987 (2020) 012020

[9] F.C. Chen, **"Introduction to Plasma Physics and Controlled Fusion"**, 2nd ed., Plenum Press (NY, 1984).

[10] A.H. Ali et al., "Using Texture Analysis Image processing Technique to Study the Effect of Microwave Plasma on the Living Tissue", *Baghdad Sci. J.*, 15 (2018) 87-97.

[11] Z.H. Shakir et al., "Influence of Cold Plasma on Sesame Paste and the Nano Sesame Paste Based on Co-occurrence Matrix", *Baghdad Sci. J.*, 19(1) (2022) 855-864.

[12] N.F. Majeed, A.H. Ali and S.N. Mazhir, "Spectroscopic Analysis of Clove Plasma Parameters Using Optical Emission Spectroscopy", *Iraqi J. Sci.*, 62(8) (2021). 2565–2570.

[13] C. Suresh, **"Textbook of Plasma Physics"**, 1st ed., CBS Pub. Distrib. Pvt. Ltd. (India, 2010).

[14] H.H. Ley, A. Yahaya and R.K.R. Ibrahim, "Analytical Methods in Plasma Diagnostic by Optical Emission Spectroscopy, A Tutorial Review", *J. Sci. Technol.*, 6(1) (2014) 49–66.

IRAQI JOURNAL OF APPLIED PHYSICS LETTERS
EDITORIAL BOARD

COPYRIGHT RELEASE FORM

IRAQI JOURNAL OF
APPLIED PHYSICS LETTERS (IJAPLett)

We, the undersigned, the author/authors of the article titled

……
……
……
……
……
……
……

that is submitted to the Iraqi Journal of Applied Physics Letters (IJAPLett) for publication, declare that we have neither taken part or full text from any published work by others, nor presented or published it elsewhere in any other journal. We also declare transferring copyrights and conduct of this article to the Iraqi Journal of Applied Physics Letters (IJAPLett) after accepting it for publication.

The authors will keep the following rights:

1. Possession of the article such as patent rights.
2. Free of charge use of the article or part of it in any future work by the authors such as books and lecture notes after informing IJAP editorial board.
3. Republishing the article for any personal purposes of the authors after taking journal permission.

To be signed by all authors:

Signature:……..date: ……
Printed name: ……

Signature:……..date: ……
Printed name: ……

Signature:……..date: ……
Printed name: ……

Correspondence author:……...
……
Address:……
……
Telephone:……..……..email: ……

Note: Complete and sign this form and mail it to the below address with your finally revised manuscript

The Iraqi Journal of Applied Physics Letters
ISSN (Print): 1999-656x, ISSN (Online): 2309-1673
www.iraqiphysicsjournal.com
Email: editor@iraqiphysicsjournal.com
Email: editor_ijap@yahoo.co.uk
Email: ijap.editor@gmail.com

IRAQI JOURNAL OF APPLIED PHYSICS LETTERS
Volume (4) Issue (3) July-September 2021

CONTENTS

About Iraqi Journal of Applied Physics Letters (IJAPLett) 1

Instructions to Authors 2

Structural Properties of Nickel Oxide Nanostructures Prepared by Induced Plasma Technique 3-6
O.A. AL Rhhauy, K.H. Razyg, K.A. Aadim

Computer-Aided Design of New Immersion Magnetic Lens 7-10
R.Y.J. AL-Salih, O.M.A. AL-Bayati

Structural Characteristics of Cadmium Oxide Thin Films Prepared by Chemical Bath Deposition 11-14
A.Y. Ali et al.

Doping of Cadmium Oxide with Chromium by Laser-Produced Plasma 15-18
B.S. Ahmed, S.J. Mohammad, G.H. Mohammed

Characterization and Antimicrobial Activity of Copper Oxide Nanoparticles 19-22
T.A. Mezher, A.M. Ali, A.N. Abd

Characterization and Parameters of Indian Costus Plasma Produced by Q-Switched Nd:YAG Laser 23-26
H.M. Abdullah, A.H. Ali

Iraqi Journal of Applied Physics Letters (IJAPLett) Copyright Form 27

Contents 28

The *Iraqi Journal of Applied Physics Letters (IJAPLett)* is a peer reviewed journal of high quality devoted to the publication of original research papers from applied physics and their broad range of applications. IJAPLett publishes quality original research letters in physics and its applications in the broadest sense. It is intended that the journal may act as an interdisciplinary forum for physics and its applications. Innovative applications and material that brings together diverse areas of physics are particularly welcome. IJAPLett aims to disseminate knowledge; provide a learned reference in the field; and establish channels of communication between academic and research experts, policy makers and executives in industry, commerce and investment institutions. IJAPLett is a quarterly specialized periodical dedicated to publishing original letters in: Applied & Nonlinear Optics, Applied Mechanics & Thermodynamics, Digital & Optical Communications, Electronic Materials & Devices, Laser Physics & Applications, Plasma Physics & Applications, Quantum Physics & Spectroscopy, Semiconductors & Optoelectronics, Solid State Physics & Applications, Alternative & Renewable Energy, and Environmental Science & Technology.

Sponsored and Published by
Iraqi Society for Alternative and Renewable Energy Sources and Techniques

Co-published by
American Quality for Scientific Publishing